Supplementary Information for

Photosensitizing Metal Covalent Organic Framework with Fast Charge Transfer Dynamics for Efficient CO_2 Photoreduction

Wang-Kang Han,[#a] Jiayu Li,[#b] Ruo-Meng Zhu,[a] Min Wei,[b] Shu-Kun Xia,[a] Jia-Xing Fu,[a] Jinfang Zhang,[a] Huan Pang,[c] Ming-De Li*[b] and Zhi-Guo Gu*[a]

[a] Key Laboratory of Synthetic and Biological Colloids, Ministry of Education, School of Chemical and Material Engineering
Jiangnan University, Wuxi 214122, China

[b] College of Chemistry and Chemical Engineering, Key Laboratory for Preparation and Application of Ordered Structural Materials of Guangdong Province
Shantou University, Shantou 515063, China

[c] School of Chemistry and Chemical Engineering
Yangzhou University, Yangzhou 225002, China

Table of Contents

Section 1. Materials and methods

1.1 Materials

All commercially available starting compounds and solvents were purchased from commercial sources and used without further purification. The organic building units 4',4''',4'''',4'''''-(ethene-1,1,2,2-tetrayl)tetrakis(([1,1'-biphenyl]-4-amine)) (ETTBA) were synthesized according to the reported procedures.[1]

1.2 General methods

Fourier transform infrared (FT-IR) spectra were collected on a Nicolet 6700 FT-IR spectrophotometer with ATR attachment. Solution ^{1}H and ^{13}C nuclear magnetic resonance (NMR) spectra were recorded on AVANCE III NMR instrument at 298 K using standard Bruker software. Solid-state ^{13}C cross-polarization magic-angle spinning (CP-MAS) NMR experiments were performed on a Bruker Avance III HD spectrometer. Electrospray ionization mass spectrometry (ESI-MS) spectra were recorded using a Waters Quattro Premier XE. Elemental analysis was collected using an Elemantar Vario EL cube under CHN model. X-ray photoelectron spectroscopy (XPS) measurements were carried out on an AXIS Supra by Kratos Analytical Inc. using monochromatized Al Ka radiation (hv = 1486.6 eV) as X-ray source. All XPS spectra were calibrated by C1s signal at 284.8 eV. Thermogravimetric analyses (TGA) were carried out using TGA/1100SF thermo grabinetric analyzer. The N_2 sorption isotherms and pore-size distribution curves were measured at 77 K using Micromeritics ASAP 2460 equipment. The CO_2 isotherms were collected up on a Micromeritics 3Flex equipment at 273 K and 298 K, respectively. The morphology and microstructure of the products were characterized by using scanning electron microscopy (SEM, HitachiS-4800) and HAADF-STEM (FEI Tecnai G2 F20). Inductively coupled plasma optical emission spectrometry (ICP-OES) measurements were carried out by using Agilent 5110. The samples were prepared via digestion by nitrohydrochloric acid, and then diluted using distilled water. Powder X-ray diffraction (PXRD) patterns were collected on a D8 Advance X-ray diffractometer (Bruker AXS Germany) with Cu $K\alpha$ radiation at room temperature. The steady-state emission experiments were performed on an Edinburgh FLSP920 spectrometer.

In situ diffuse reflectance infrared Fourier transform spectroscopy (DRIFTS) measurements were performed using a Nicolet iS50 spectrometer (Thermo, USA). Fourier-transform spectrometer equipped with a Harrick diffuse reflectance accessory at the Infrared Spectroscopy. The chamber was sealed with two ZnSe windows. First, the silicon crystal was polished. Briefly, an appropriate amount of 0.5 um alumina polishing powder was poured

onto the polishing machine, and an appropriate amount of ultrapure water was added to make it evenly distributed, and rough polishing was performed at a rotational speed of about 300. Then, the above process was repeated and the polishing table was thoroughly cleaned before being polished with 0.05 um silicon oxide polishing powder to achieve a smooth finish. The polished silicon crystal was put into a 50 ml beaker and sequentially sonicated with ultrapure water and ethanol for 5 min and rinsed with ultrapure water to obtain the polished silicon crystal. The sample was prepared as follows: 5 mg of photocatalysts was dispersed in 225 uL of ethanol and 25 μL of Nafion by ultrasonication. Then, 30 uL of the resulting suspension was uniformly added dropwise to the silicon crystal and dried under an infrared lamp. Then, 5 mL of MeCN with 0.2 mL TEOA and 0.02 M of BIH were added. The reaction cell was filled with ultra-pure CO_2 gas and connected to the IR instrument. Finally, the light was turned on, and the in-situ DRIFTS data were collected. The spectrum at 0 min in light was recorded as a background.

The single-crystal X-ray data of Ru-bpm was collected on a Bruker APEX-II CCD diffractometer with graphite monochromatic Mo $K\alpha$ radiation (λ = 0.71073 Å). The data was collected at 296 K. Using *Olex2*,[2] the crystal structures were solved with the *ShelXT*[3] structure solution program using Intrinsic Phasing and refined with the *ShelXL*[4] refinement package using Least Squares minimization. All of the non-hydrogen atoms except the anions were refined with anisotropic thermal displacement coefficients. Hydrogen atoms of organic ligands were located geometrically and refined in a riding model.

The fs-TA measurements were performed based on a femtosecond Ti: Sapphire regenerative amplifier laser system (Coherent, Astrella-Tunable-F-1k) and femtosecond transient absorption spectrometer system (Ultrafast Systems, Helios Fire). The laser probe pulse was produced with ~4% of the amplified 800 nm laser pulses to generate a white-light continuum (320-800 nm) in a CaF2 crystal and then this probe beam was split into two parts before traversing the sample. One probe laser beam with spot size 7.9×10-9 m^2 goes through the sample, while the other probe laser beam goes to the reference spectrometer to monitor the fluctuations in the probe beam intensity. The instrument response function was determined to be ca. 120 fs. At each temporal delay, data were averaged for 1 s and collected by the acquisition system. For the experiments described in this study, the sample solution was excited by a 350 nm pump beam with a power of 0.5 mW (63.2 μJ/cm^2) (from TOPAS). The sample solutions were excited in a 2 mm path-length cuvette with a stir bar. The data were stored as three-dimensional (3D) wavelength-time-absorbance matrices that were exported for use with the fitting software. Chirp correction was done for all the data shown here. The kinetics of all fs-TA spectra were fitted by single-wavelength fitting via Surface Xplorer software.

Section 2. General synthetic procedures and characterizations

2.1 Synthesis and characterizations of Ru-bpm

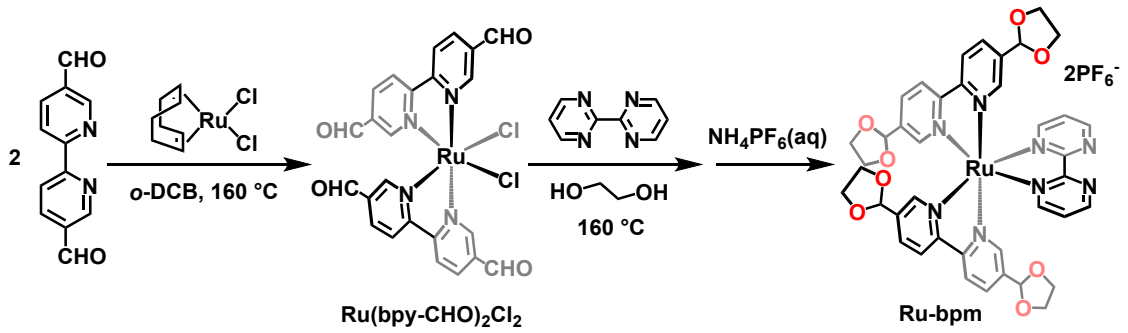

The synthesis of metal complex Ru-bpm was as follow: $Ru(bpy\text{-}CHO)_2Cl_2$ was synthesized according to our previous work.[5] Typically, in a 50 mL round bottom flask, $Ru(bpy\text{-}CHO)_2Cl_2$ (596.4 mg, 1 mmol) and 2,2'-bipyrimidine (189.79 mg, 1.2 mmol) were suspended in 25 mL of ethylene glycol. The mixture was heated at 160 °C for 72 h with rapid stirring under Ar atmosphere and was then cooled to room temperature. Then, a saturate solution of NH_4PF_6(aq) was added and the orange-red precipitate of the desired compound appeared quickly. The orange-red precipitate was filtered, washed with cold water and diethyl ether, then dried under vacuum. Yield: 68%. The orange-red crystal was obtained by slow diffusion of diethyl ether into the CH_3CN solution of Ru-bpm at room temperature. Notably, during the reaction, the aldehyde groups were protected by the ethylene glycol molecules to form the acetal product. This acetalization may be catalyzed by the ruthenium(III) trichloride.[6] ^{1}H NMR (400 MHz, CD_3CN, δ: ppm) 9.14 (m, 2H), 8.57 (q, 4H), 8.20 (m, 4H), 8.05 (q, 2H), 7.84 (d, 2H), 7.63 (m, 4H), 5.72 (d, 4H), 3.96 (m, 16H). ^{13}C NMR (101 MHz, CD_3CN, δ: ppm) 163.72, 160.47, 158.93, 157.73, 150.90, 150.30, 139.60, 137.10, 125.30, 100.37, 66.03. ESI-MS, m/z Calcd. for $C_{40}H_{38}F_{12}N_8O_8P_2Ru$ $[M\text{-}PF_6]^+$ 1005.2, found: 1005.2; $[M\text{-}2PF_6]^{2+}$ 430.1, found 430.1.

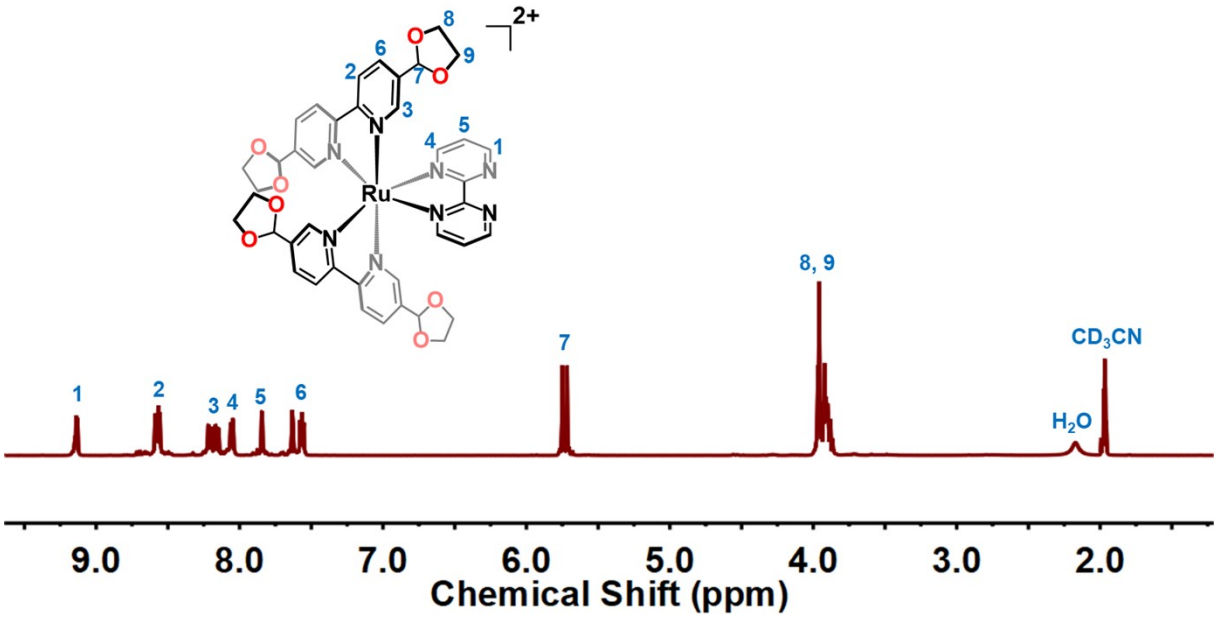

Figure S1. ^{1}H NMR spectrum of Ru-bpm.

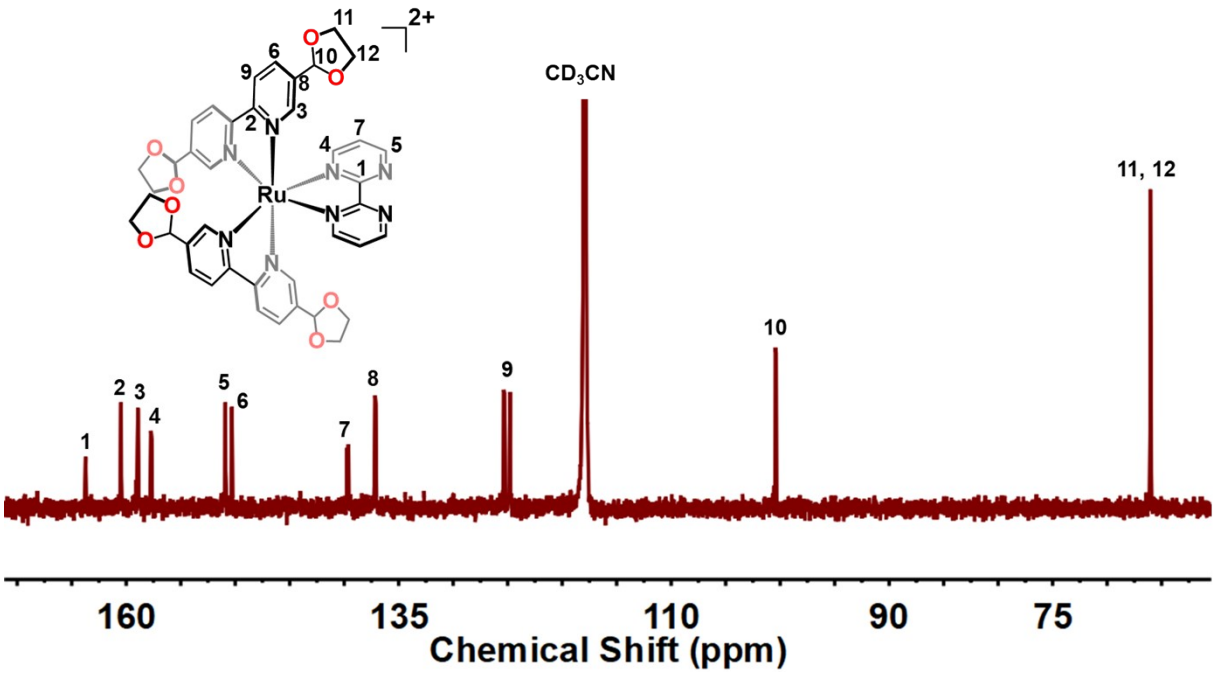

Figure S2. ^{13}C NMR spectrum of Ru-bpm.

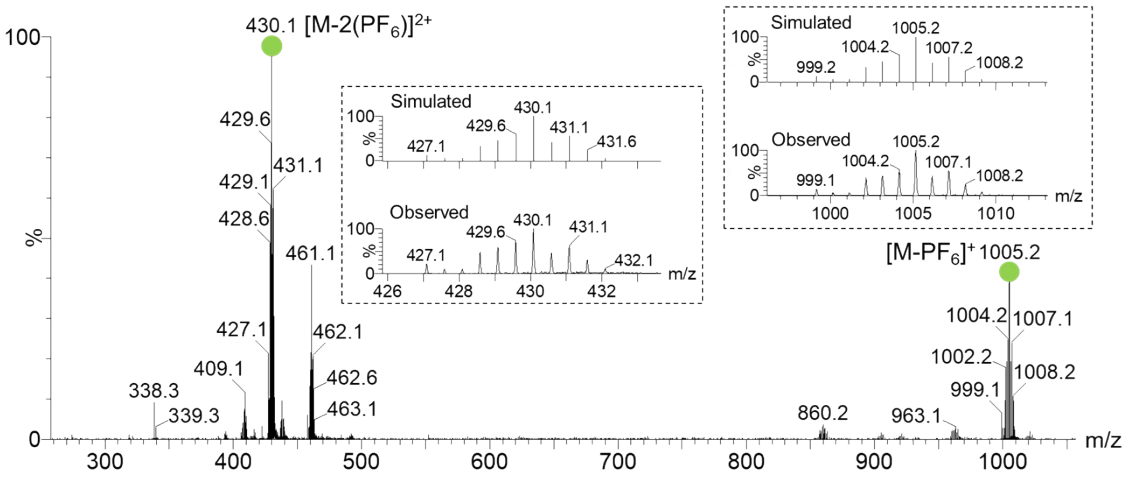

Figure S3. ESI-MS spectrum of Ru-bpm. Insert: the observed and simulated +1 and +2 isotopic peak distributions, respectively.

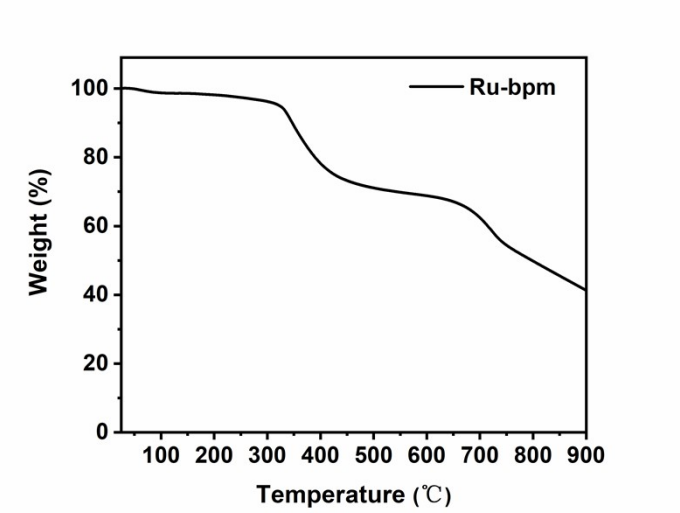

Figure S4. Thermogravimetric analysis of Ru-bpm.

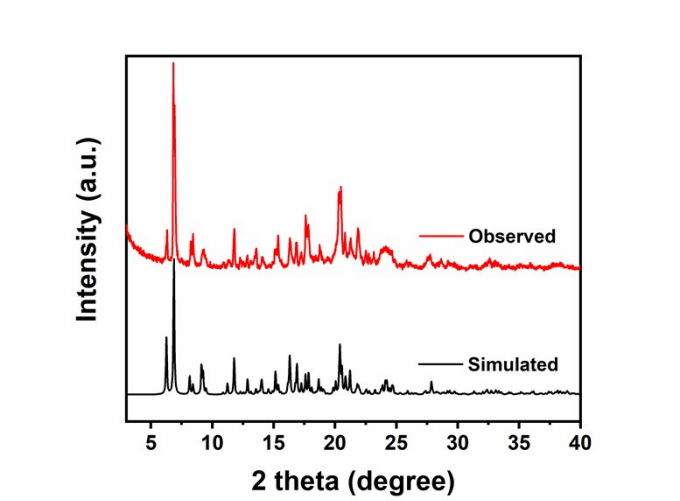

Figure S5. Powder X-ray diffraction of the as-synthesized sample and single-crystal simulation of Ru-bpm, confirming the phase purity of our sample.

2.2 X-ray single crystal structure of Ru-bpm

Single-crystal X-ray diffraction data reveals that Ru-bpm crystallizes in the triclinic *P*-1 space group. The Ru(II) centre is in a typical octahedral geometry. Each Ru(II) coordinate with two bipyridine derived ligands and one 2,2'-bipyrimidine ligand, forming an octahedral RuN_6 coordination geometry. Two PF_6^- counter anions balance the charge. The single crystal structure clearly showed that the four aldehyde groups were protected by four ethylene glycol molecules, respectively, to form the acetal product. The remaining N coordination site in 2,2'-bipyrimidine ligand can coordinate other metal ions, such as Re(I) in this work. The crystal structure proved that Ru-bpm can be used as a 4-connected building unit for constructing MCOFs. Final crystallographic data for Ru-bpm is listed in Table S1. CCDC: 2323722.

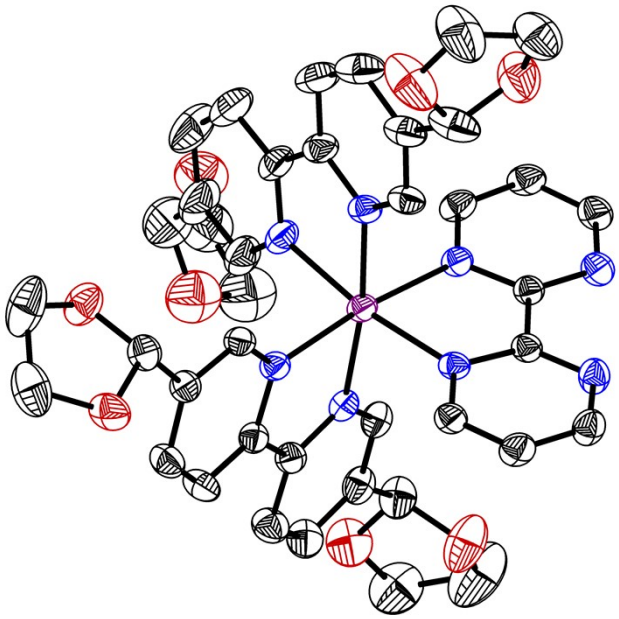

Figure S6. The single crystal X-ray structure for Ru-bpm (ORTEP, 30% ellipsoids). All H atoms and solvent molecules have been removed for clarity (C: Grey; N: blue; Ru: purple; O: red).

Table S1 Summary of crystallographic data for Ru-bpm.

Ru-bpm	
Formula	$C_{40}H_{38}F_{12}N_8O_8P_2Ru$
Formula Weight	1149.79
T (K)	296 K
λ (Å)	0.71073
Crystal system	triclinic
Space group	P-1
a (Å)	13.1278(11)
b (Å)	13.7431(11)
c (Å)	14.5832(13)
α (^{0})	86.847(3)
β (^{0})	75.173(3)
γ (^{0})	69.277(3)
V (Å^3)	2377.1(4)
Z	2
D_{calc} (g/cm^3)	1.606
Mμ (mm^{-1})	0.503
F(000)	1160
θ (^{0})	1.943 - 27.524
Index ranges	-17 <= h <= 17 -17 <= k <= 17 -18 <= l <= 13
Reflections collected	8288
GOF (F^2)	1.024
R_1[a],wR_2[b](I>2σ(I))	0.0665, 0.1814
R_1[a],wR_2[b](all data)	0.0871, 0.1998

$R_1{}^a = \Sigma||F_o| - |F_c||/\Sigma|F_o|$. $wR_2{}^b = [\Sigma w(F_o{}^2 - F_c{}^2)^2/\Sigma w(F_o{}^2)]^{1/2}$

2.3 The model reaction

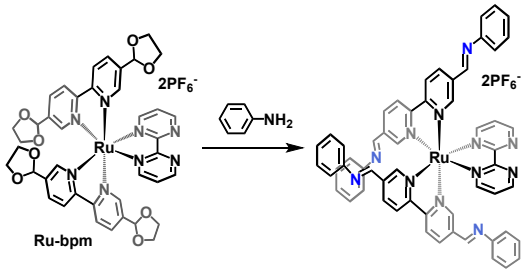

The metal complex building unit Ru-bpm (22.99 mg, 0.02 mmol) and aniline (7.45 mg, 0.08 mmol) were dissolved in a mixed solvent of 0.6 mL *o*-DCB, 0.4 mL *n*-BuOH, and 0.15 mL 6M aqueous acetic acid in a pyrex tube. Then, the pyrex tube was flash frozen in a liquid N_2 bath and degassed by freeze-pump-thaw technique for three times and sealed under vacuum. Upon warming to room temperature, the tube was placed in an oven and heated at 120 °C for 12 hours. After cooling to room temperature, orange solid was formed on the bottom of the pyrex tube, which was filtered and dissolved in CH_3CN for the analysis of ESI-MS.

The ESI-MS spectrum showed ion peaks at m/z = 1129.2 and 492.1, corresponding to +1 and +2 ion peaks of the model compound, respectively (Figures S7 and S8). This result clearly confirmed that the Ru-bpm building unit is stable in the above solvothermal condition. Besides, the ESI-MS spectra also showed ion peaks of the corresponding intermediate products which were agreed very well with the simulated isotopic patterns, indicating the in situ sequential deprotection and imine condensation process in the reaction.

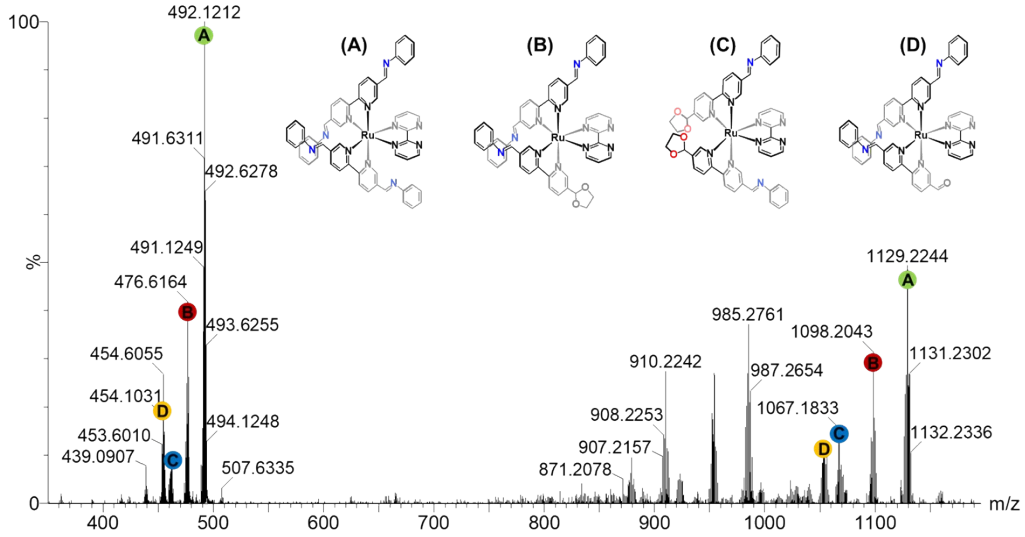

Figure S7. The ESI-MS spectra for the isolated product of the model reaction.

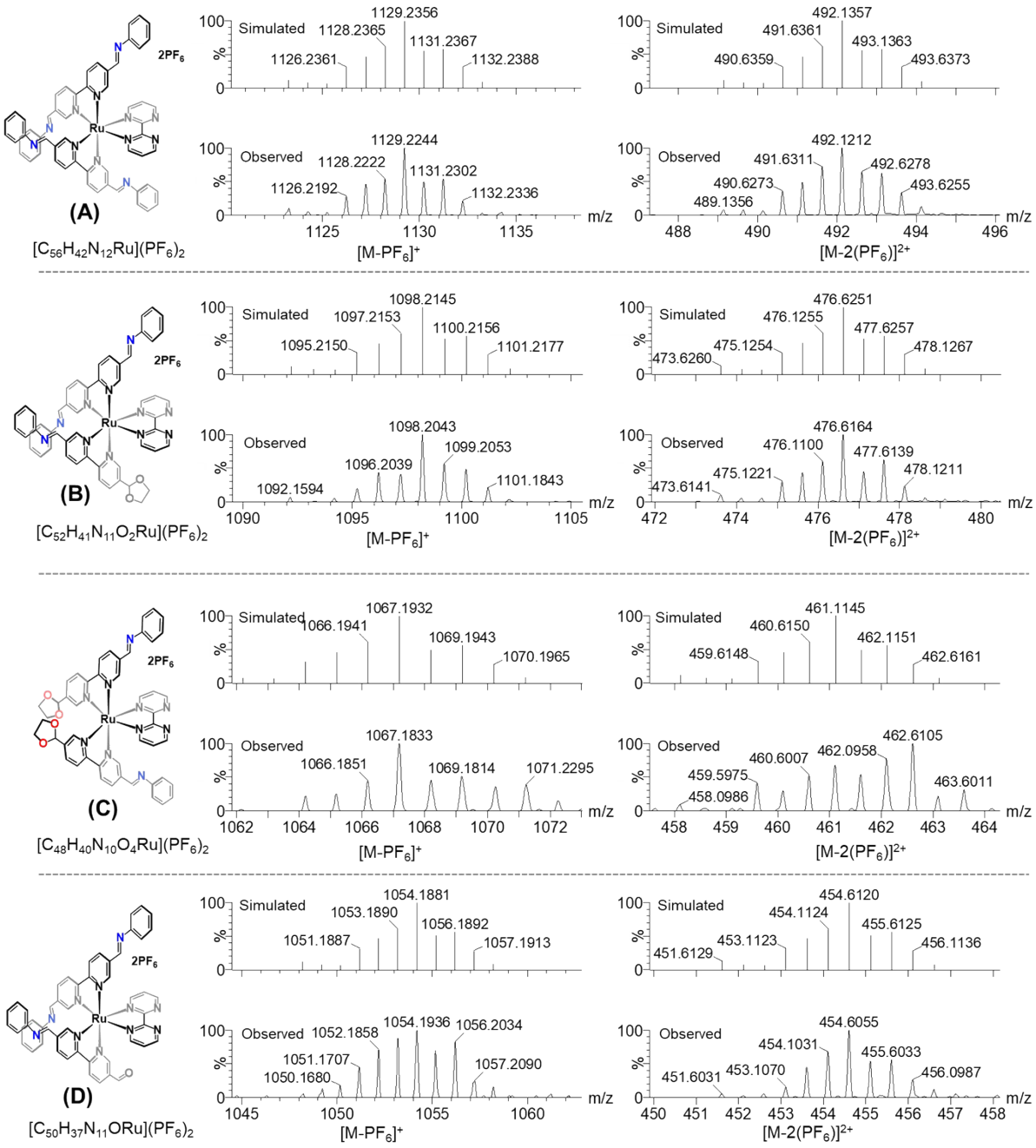

Figure S8. The observed and simulated isotopic peak distribution showing the corresponding +1 and +2 ion peaks.

2.4 Synthesis of MCOFs

The synthesis of MCOF-Ru: The MCOF-Ru was synthesized by solvothermal condensation reaction. In a pyrex tube, Ru-bpm (22.99 mg, 0.02 mmol) and ETTBA (13.94 mg, 0.02 mmol) were dissolved in a mixed solvent of 0.6 mL *o*-DCB, 0.4 mL *n*-BuOH, and 0.15 mL 6M aqueous acetic acid. The above mixture was sonicated for 10 min to get a homogeneous dispersion. Then, the pyrex tube was flash frozen in a liquid N_2 bath and degassed by freeze-pump-thaw technique for three times and sealed under vacuum. Upon warming to room temperature, the tube was placed in an oven and heated at 120 °C for 4 days. The precipitate was collected by filtration, washed with DMF (8 × 5 mL), extracted by Soxhlet extractor with THF for 24 hours, and finally dried at 90 °C under vacuum overnight to obtain brownish red crystalline powder. Yield: 76%. Elemental analysis of MCOF-Ru: Calcd. for $C_{328}H_{216}N_{48}Ru_4P_8F_{48}$: C, 61.62%; H, 3.41%; N, 10.51%. Found: C, 62.73%; H, 3.56%; N, 10.07%.

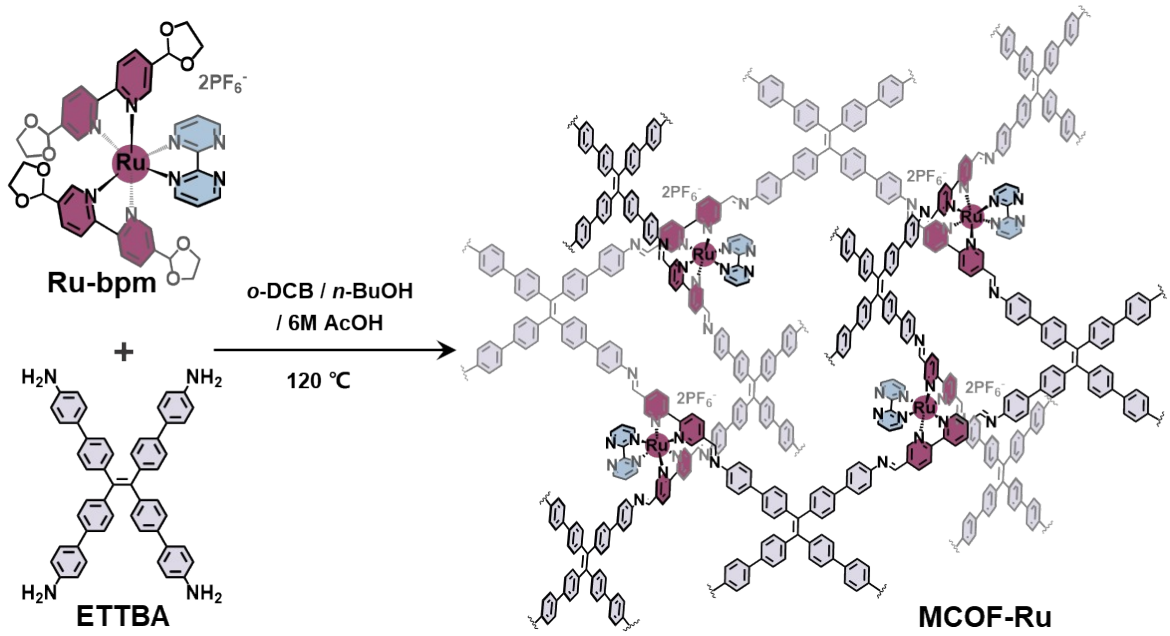

Figure S9. Illustration of the synthetic procedure for MCOF-Ru.

The synthesis of MCOF-Ru/Re: The MCOF-Ru/Re was synthesized through the post modification method. MCOF-Ru (100 mg) and $Re(CO)_5Cl$ (45 mg) were dispersed in 50 mL toluene, reflux 60 mins while stirring. After cooling to room temperature, the products were filtered and washed with methanol and diethyl ether. And finally dried at 60 °C under vacuum for 6 hours to obtain brownish red crystalline powder. Yield: 96%. The Re content in MCOF-Ru/Re was determined by ICP-OES to be 6.52 wt%, suggesting that about 56% of the reserved coordination sites on 2,2'-bipyrimidine ligands were converted to Re(I) sites.

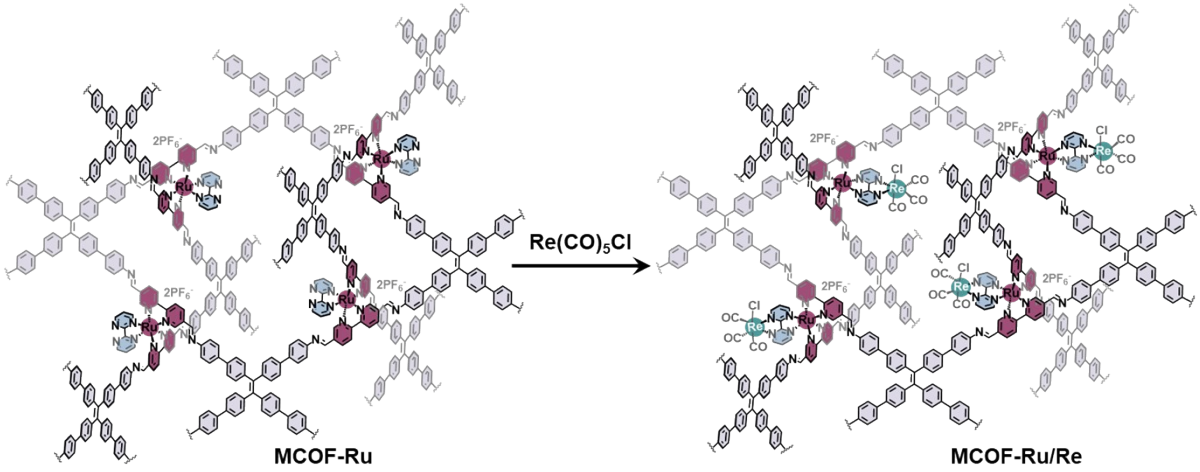

Figure S10. Illustration of the synthetic procedure for MCOF-Ru/Re

2.5 FT-IR analysis

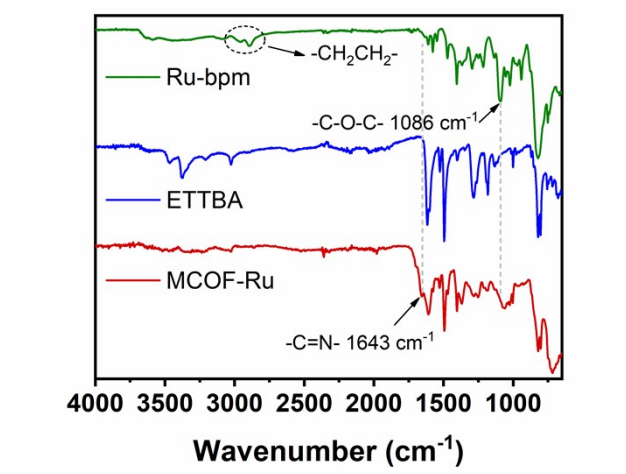

Figure S11. FT-IR spectra of Ru-bpm, ETTBA and MCOF-Ru.

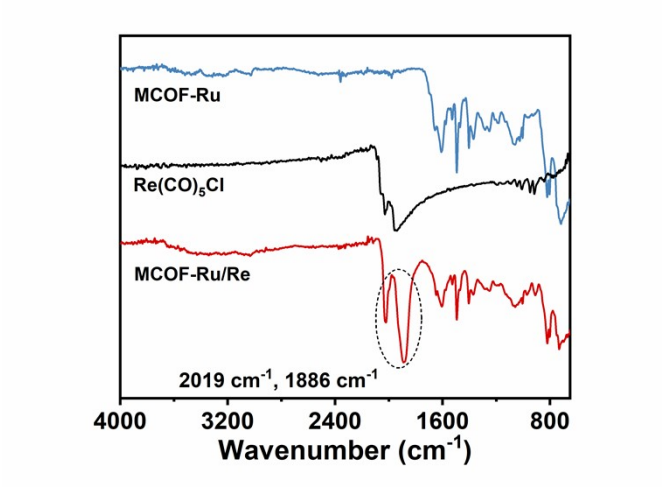

Figure S12. FT-IR spectra of MCOF-Ru and MCOF-Ru/Re. As for MCOF-Ru/Re, two additional peaks arise at 2019 and 1886 cm^{-1} can be observed, which can be attributed to the C≡O stretching vibration of the Re(I) moieties.

The as-synthesized materials were characterized by FT-IR. Compared with the building units, the -CH_2- (2890-2960 cm^{-1}) and -C-O-C- (1086 cm^{-1}) from Ru-bpm segment and N-H stretching vibration (3250-3450 cm^{-1}) from ETTBA amine were disappeared for MCOF-Ru. Meanwhile, the characteristic C=N stretching vibration was appeared at around 1643 cm^{-1}. The FT-TR results indicated that the *in situ* deprotection and polymerization occurred with the formation of imine linkages.

2.6 Solid-state ^{13}C NMR spectra

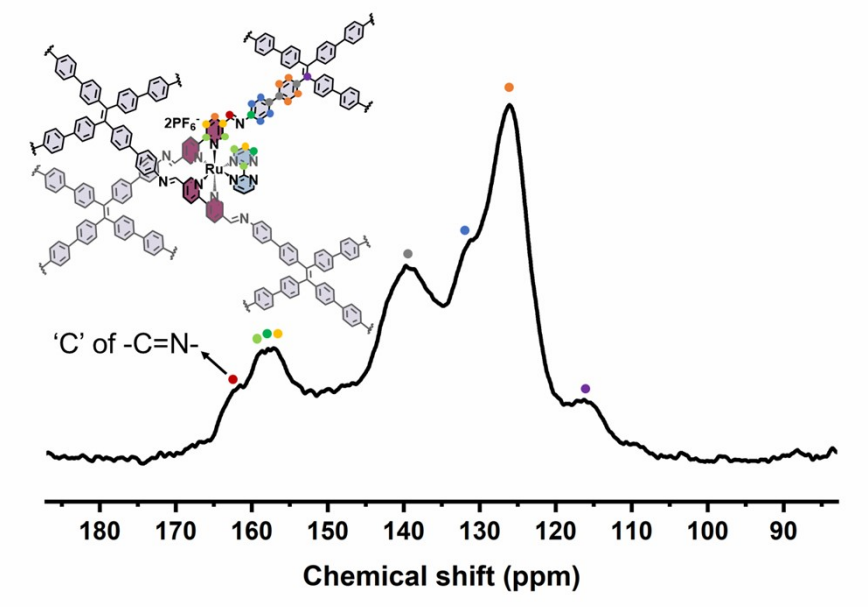

Figure S13. ^{13}C solid-state NMR spectrum of MCOF-Ru.

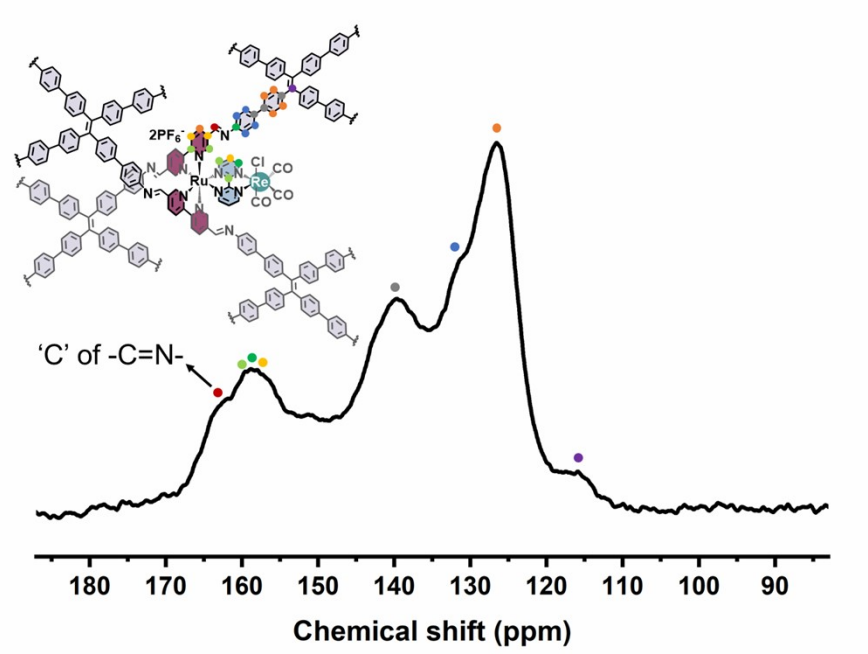

Figure S14. ^{13}C solid-state NMR spectrum of MCOF-Ru/Re.

The as-synthesized material was characterized by ^{13}C solid-state NMR spectra. The appearance of characteristic resonance peak of imine carbon (161.8 ppm for MCOF-Ru, 162.7 ppm for MCOF-Ru/Re) suggested the successful formation of imine linkage. Besides, the signals of benzene, bipyridine and bipyrimidine units appeared between 160 and 110 ppm.

2.7 Thermogravimetric analysis

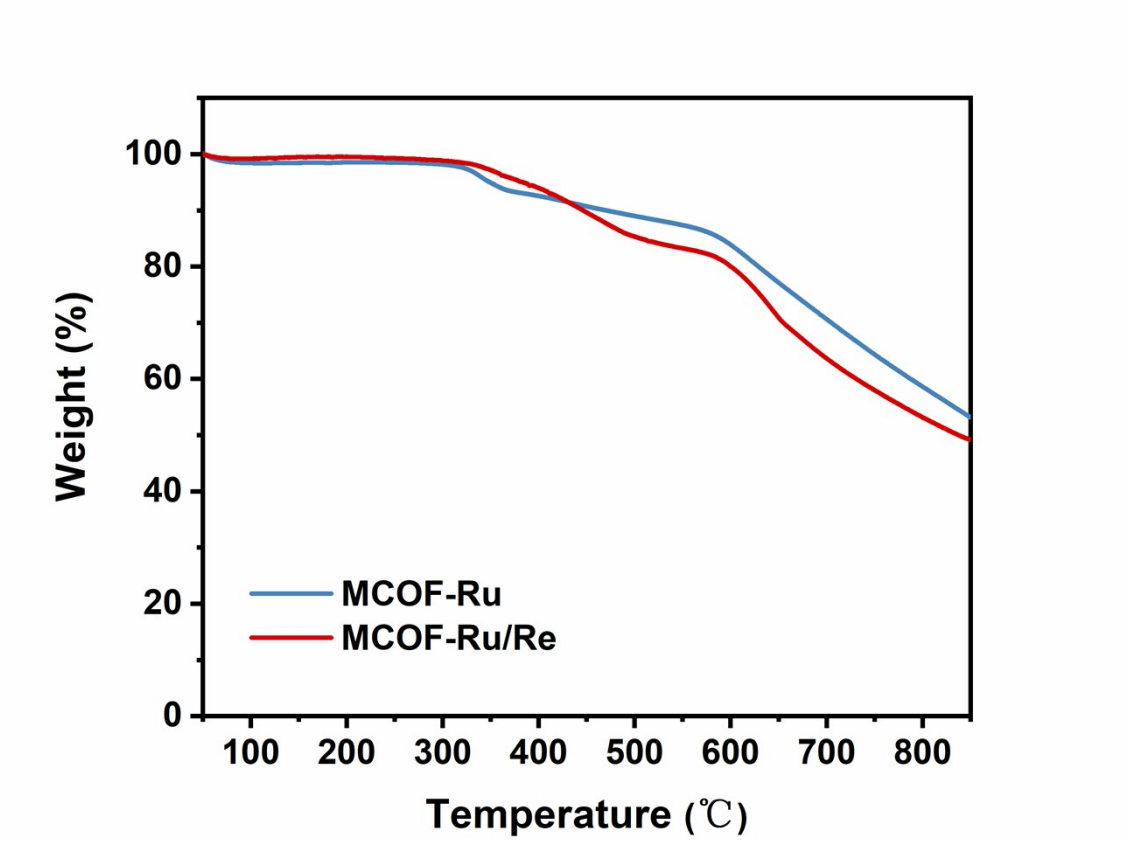

Figure S15. TGA profiles of MCOFs showed that both of the two MCOFs was thermally stable up to about 320 ℃.

2.8 N_2 adsorption-desorption measurement

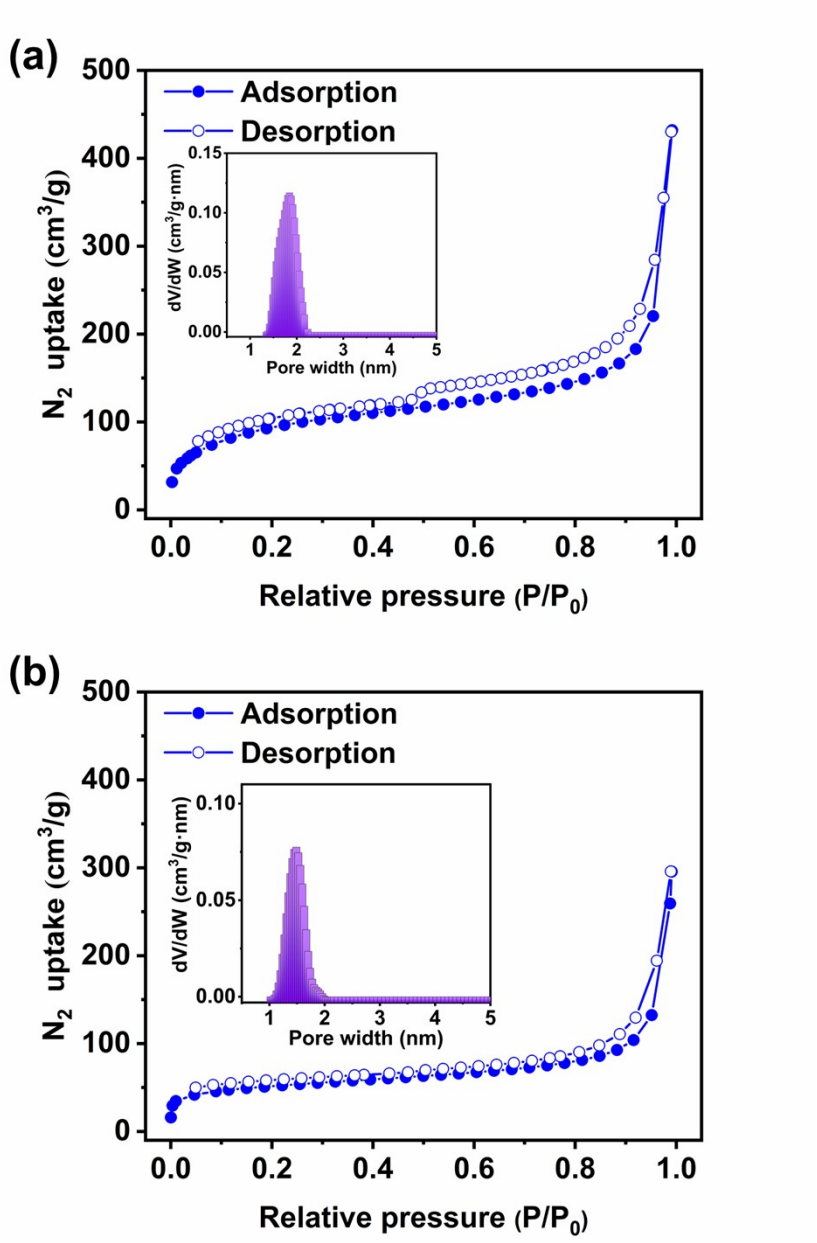

Figure S16. N_2 adsorption/desorption isotherms with pore size distributions of (a) MCOF-Ru and (b) MCOF-Ru/Re.

The porous structures of the MCOFs were analyzed by N_2 adsorption-desorption measurements. The N_2 Brunauer-Emmett-Teller (BET) surface areas of MCOF-Ru and MCOF-Re were calculated to be 328 and 175 m^2g^{-1}, respectively. The moderate N_2 adsorption is mainly attributed to the blockage of channels by the bulky PF_6^- anions. Similar phenomena have been observed in other porous materials that the bulky anions or other guest molecules not only block the pore but also reduce the pore size. The NLDFT pore size distribution analysis showed that the pore size of about 1.82 and 1.46 nm for MCOF-Ru and MCOF-Ru/Re, respectively.

2.9 SEM, TEM and XPS analysis

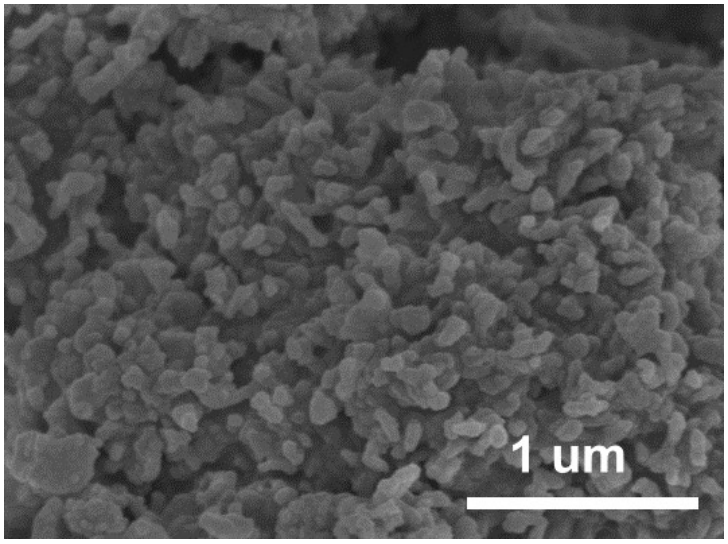

Figure S17. SEM image of MCOF-Ru.

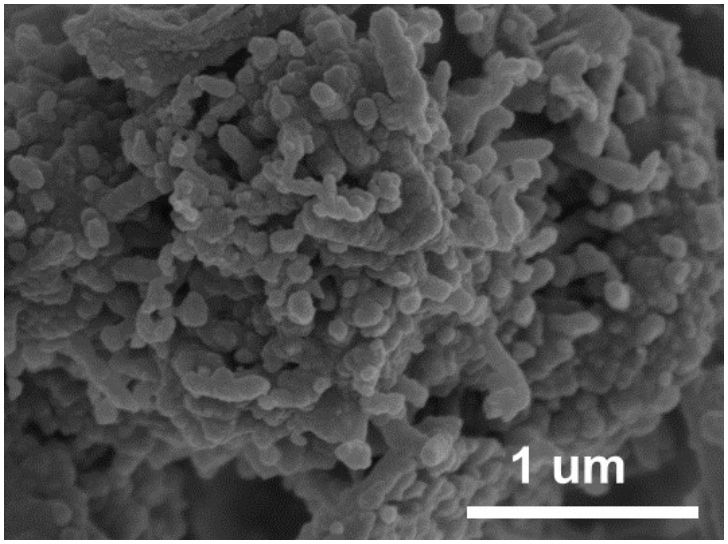

Figure S18. SEM image of MCOF-Ru/Re.

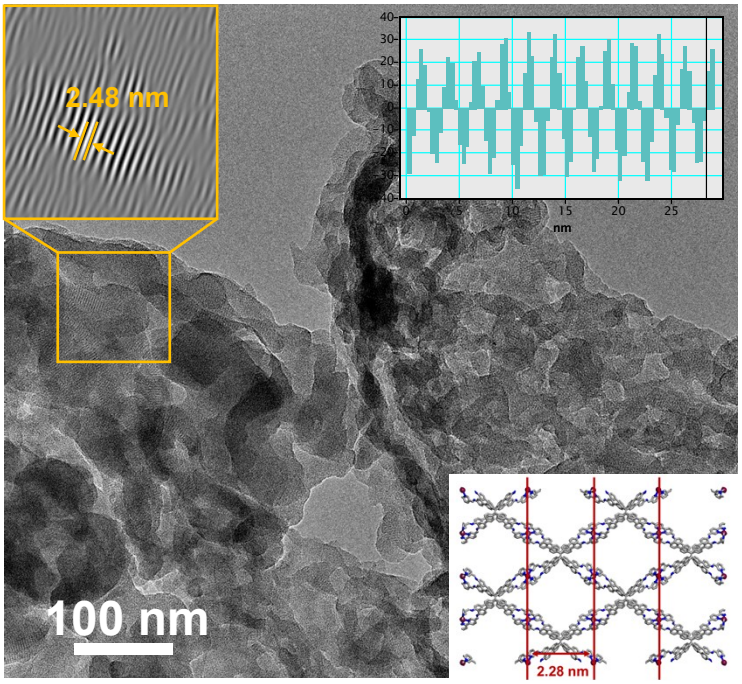

Figure S19. HRTEM image of MCOF-Ru. Insets: Fourier-filtered image of the selected region. The structural model of MCOF-Ru takes along the [001] direction. All H atoms have been removed for clarity (C: Grey; N: blue; Ru: purple). The HRTEM image with clear lattice fringes demonstrated the crystalline structure of the as-synthesized MCOF-Ru. The *d*-spacing value was 2.48 nm, which was close to the theoretical distance (2.28 nm) between Ru-to-Ru in our proposed structure taking along the [001] direction. The HRTEM result further confirmed the rationality of the simulated structure.

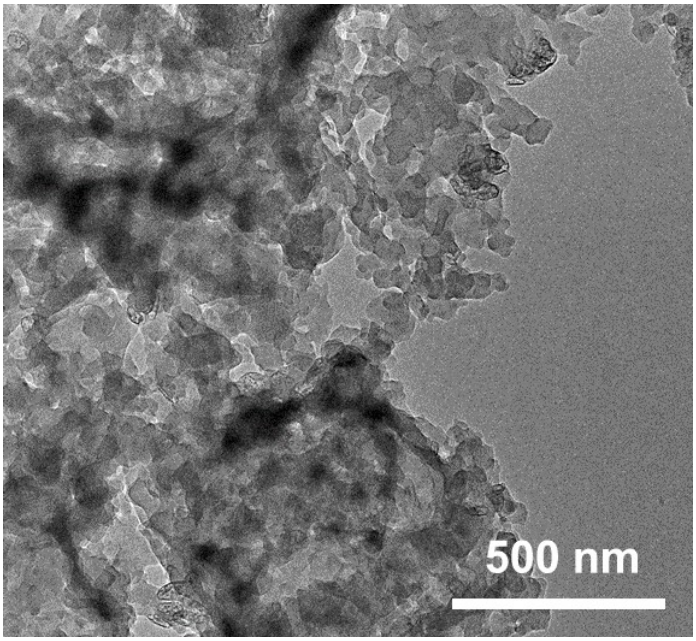

Figure S20. HRTEM image of MCOF-Ru/Re. Unfortunately, no lattice fringe was observed since the material was sensitive to electron beam.

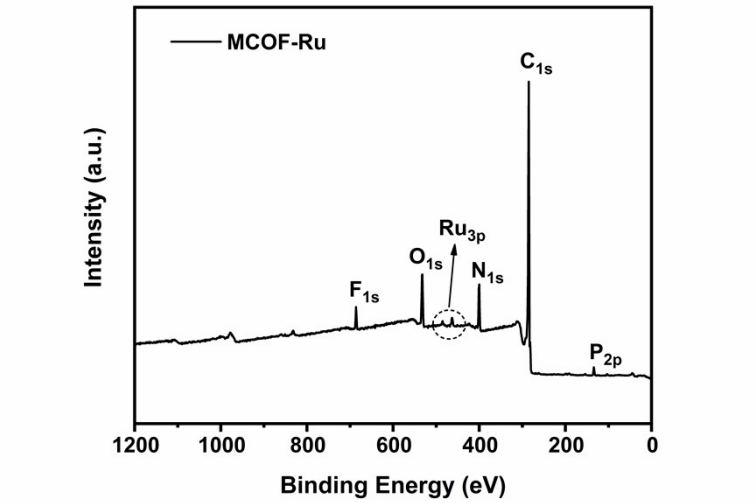

Figure S21. XPS survey spectrum of MCOF-Ru.

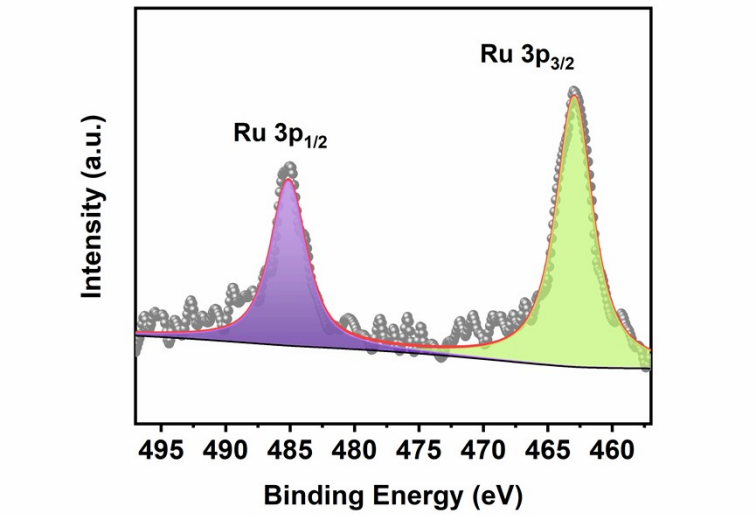

Figure S22. The high-resolution XPS spectrum of MCOF-Ru for region Ru 3p.

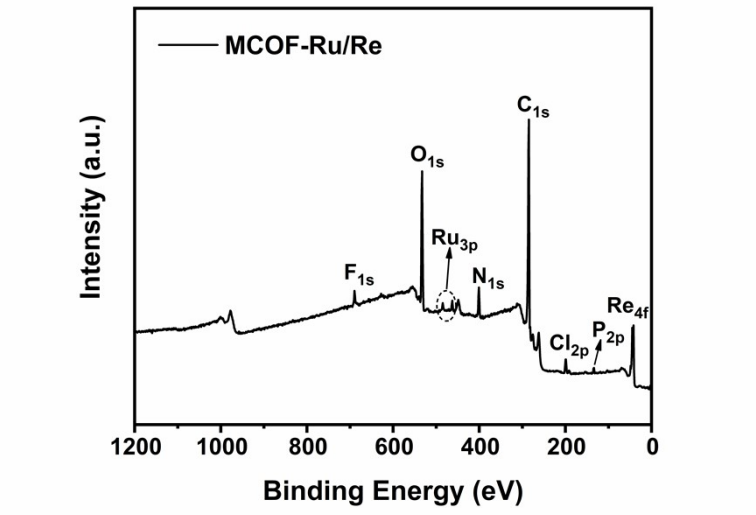

Figure S23. XPS survey spectrum of MCOF-Ru/Re.

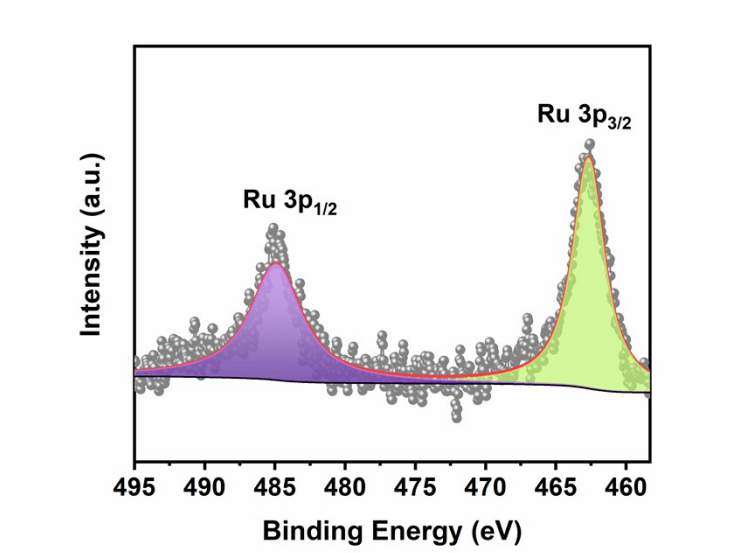

Figure S24. The high-resolution XPS spectrum of MCOF-Ru/Re for region Ru 3p.

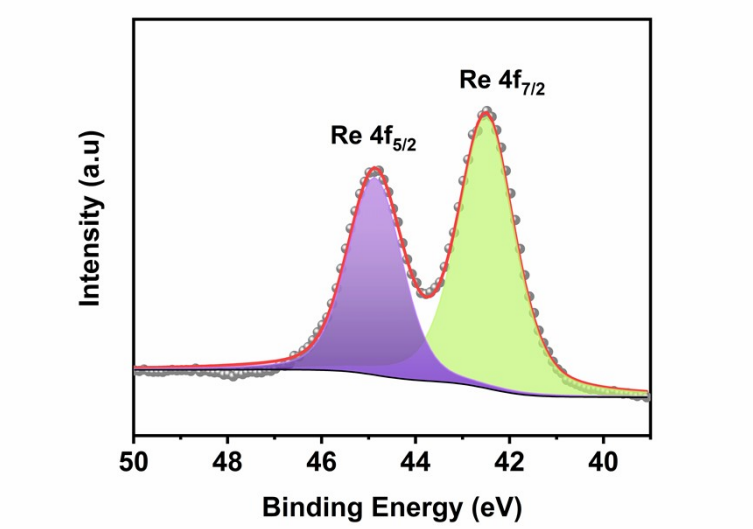

Figure S25. The high-resolution XPS spectrum of MCOF-Ru/Re for region Re 4f.

The XPS was performed to explore the metal valence states in MCOFs. For MCOF-Ru, the high-resolution XPS spectrum showed the binding energy of the Ru element for $3p_{1/2}$ and $3p_{3/2}$ are at 484.9 and 462.7 eV, respectively, suggested the presence of Ru(II) species.[7] Similarly, MCOF-Ru/Re also showed the binding energy at 485.0 and 462.9 eV for Ru $3p_{1/2}$ and Ru $3p_{3/2}$, respectively. Besides, in the XPS spectrum of Re 4f for MCOF-Ru/Re, the peaks at 44.6 and 42.1 eV are assigned to Re $4f_{5/2}$ and $4f_{7/2}$ levels of the coordinated Re(I) species, respectively.[8,9]

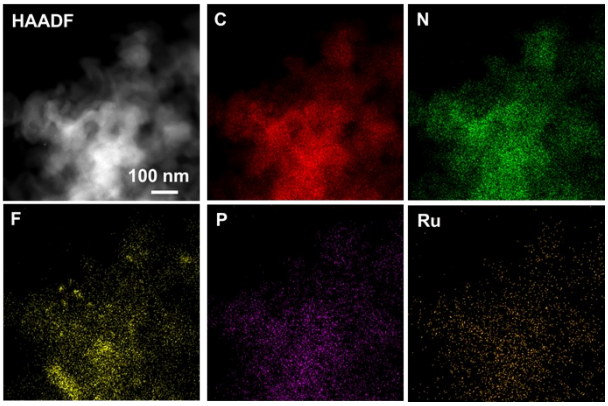

Figure S26. The elemental mapping images of MCOF-Ru.

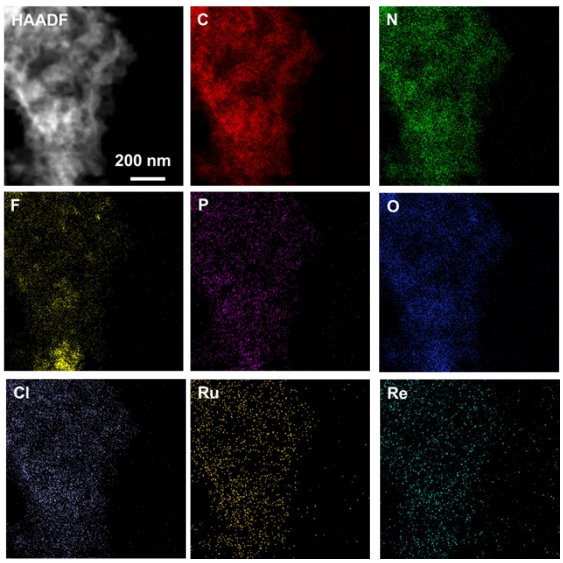

Figure S27. The elemental mapping images of MCOF-Ru/Re.

Section 3. PXRD analysis and structural modeling of the MCOFs

3.1 Comparison of PXRD patterns for MCOFs and their related monomers

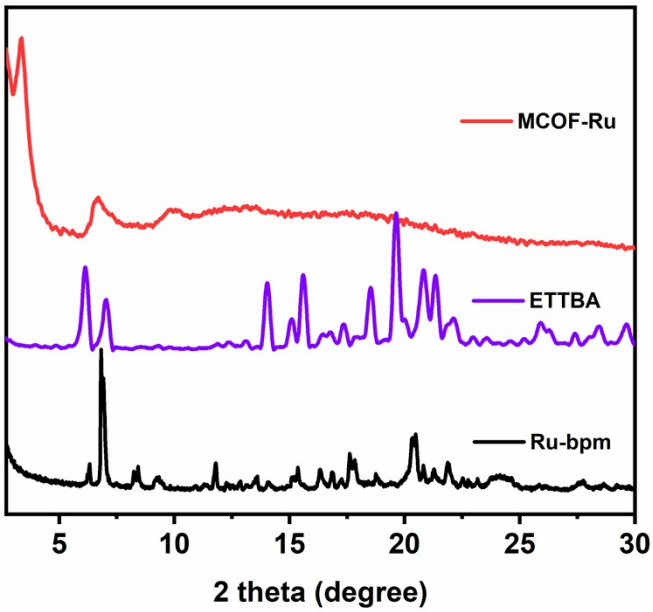

Figure S28. The comparison of experimental PXRD patterns for MCOF-Ru and its starting monomers, ETTBA and Ru-bpm. The MCOF-Ru showed distinct reflections with respect to both starting monomers.

3.2 Structural modeling of the MCOFs

Molecular modeling was conducted with the Materials Studio (ver. 8.0) program. Considering the geometry of the precursors and the connection patterns, we constructed models for each of the possible structures (*eg*. 2D **sql** net, and 3D **lvt**, **ssb** nets), and compared their simulated PXRD patterns with the experimental data. The vertex positions were obtained from Reticular Chemistry Structure Resource (RCSR) database for structural modeling.[10] The structural models were geometrically optimized using MS Forcite molecular dynamics module method. Pawley refinement was carried out using Reflex software package. The Pawley refinements were performed to optimize the lattice parameters iteratively until the R_p and R_{wp} value converges and the overlay of the observed with refined profiles showed good agreement.

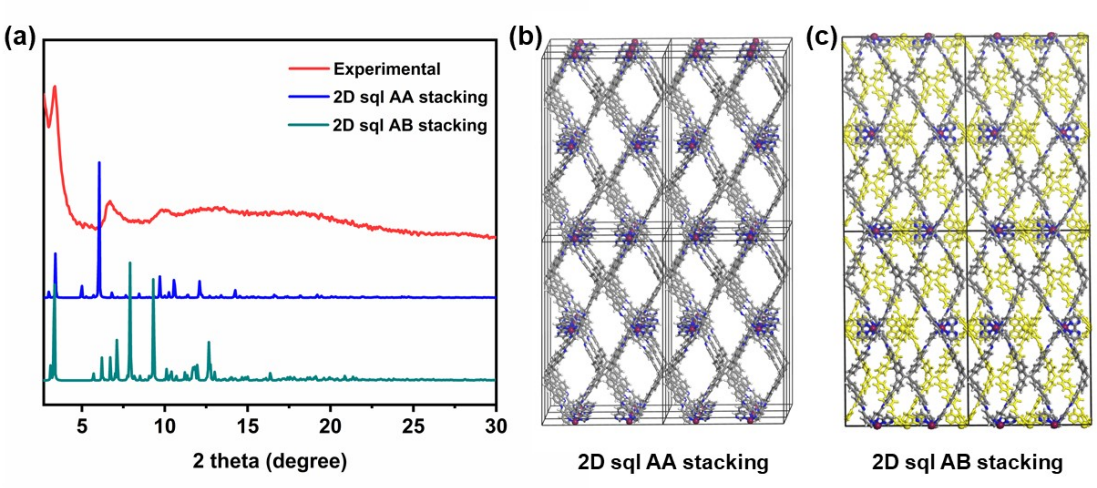

Figure S29. Simulated PXRD pattern and structure of MCOF-Ru with 2D **sql** topology. (a) experimental (red) and simulated PXRD patterns for AA (blue) and AB (green) stacking, respectively. The corresponding structure of (b) AA stacking and (c) AB stacking. AA stacking: space group *P*2, a = 9.47 Å, b = 35.47 Å, c = 53.77 Å, α = 90°, β = 105.34°, γ = 90°. AB stacking: space group *P*2, a = 15.66 Å, b = 32.98 Å, c = 54.94 Å, α = 90°, β = 107.86°, γ = 90°.

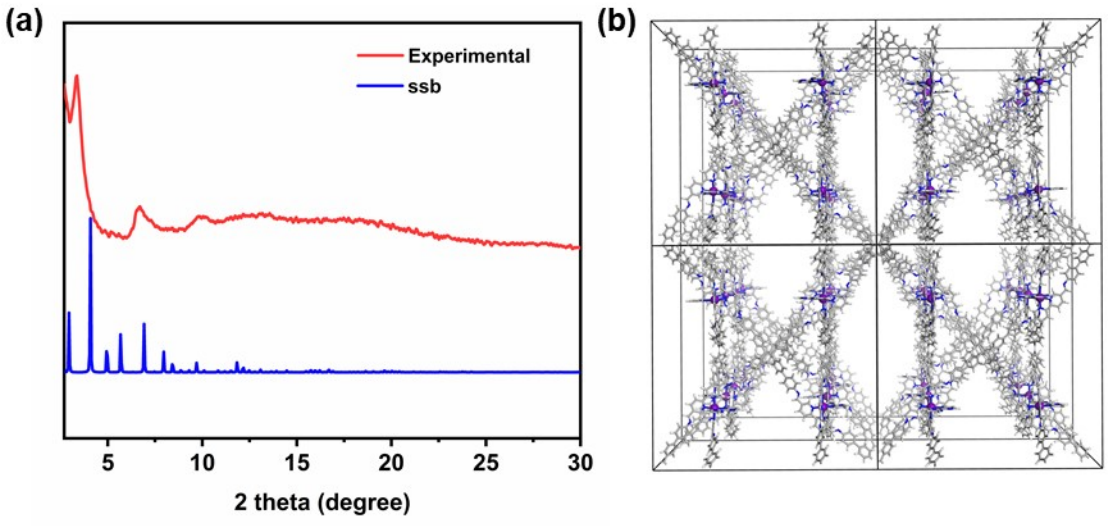

Figure S30. Simulated PXRD pattern and structure of MCOF-Ru with **ssb** topology. (a) experimental (red) and simulated PXRD patterns (blue). (b) The corresponding structure of **ssb** net built from Ru(bpm)$(PF_6)_2$ and ETTBA. Space group *I*222, $a = b = c$ = 45.35 Å, $\alpha = \beta = \gamma$ = 90°.

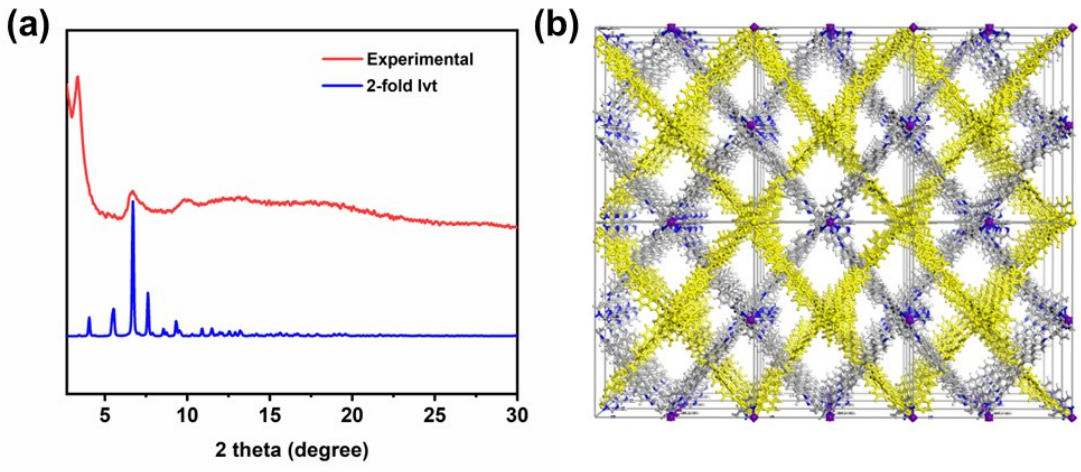

Figure S31. (a) Experimental (red) and simulated PXRD patterns (blue) of MCOF-Ru with 2-fold interpenetrated **lvt** topology. (b) The corresponding structure. Space group *Pnc*2, a = 33.36 Å, b = 45.62 Å, c = 33.63 Å, $\alpha = \beta = \gamma$ =90°.

Section 4. Photocatalysis experiments

4.1 Calculation process of optical band gaps

The optical band gap energy (E_g) can be estimated by assuming direct transitions between valence and conduction bands with the following relation[11,12]

$$(\alpha hv)^2 = C\,(hv - E_g)$$

where α is absorption coefficient, hv is the incident photo energy, and C is a proportionality constant. Linear behavior exists in a certain range of Tauc plots ($(\alpha hv)^2$ versus hv), supporting the assumption of direct transitions for the two MCOFs. The optical band gap E_g can be obtained by extrapolating the linear portion of the plot relating $(\alpha hv)^2$ and hv to $(\alpha hv)^2 = 0$.

4.2 Photoelectrochemical measurement

Photoelectrochemical and electrochemical measurements including Mott-Schottky plots, photocurrent-time (I-t) profiles and electrochemical impedance spectra (EIS) were recorded on the CHI660E electrochemical workstation via a three-electrode system with the photocatalyst-coated ITO as the working electrode, Pt plate as the counter electrode and the Ag/AgCl electrode (saturated KCl) as the reference electrode. The working electrodes were prepared as follows: COF powder (5.0 mg), 10.0 μL of Nafion (5 wt%, dispersed in water) and dry ethanol (0.5 mL) was ultrasonicated for 1 h to form a homogeneous suspension. Then, 200 μL suspension was dropped onto an ITO glass substrate and dried at room temperature. A 0.5 M Na_2SO_4 solution was used as the electrolyte. Irradiation conditions were the same as photocatalytic tests. The applied potentials vs. Ag/AgCl is converted to RHE potentials using the following equation:

$$E_{RHE} = E_{Ag/AgCl} + 0.0591\text{pH} + E^{\theta}_{Ag/AgCl}\ (E^{\theta}_{Ag/AgCl} = 0.199\ \text{V})$$

The curves of Mott-Schottky measurements showed positive slopes, corresponding to the n-type semiconductor character of the MCOFs. The flat band potential (E_{fb}) at -0.69 and -0.82 (V vs Ag/AgCl) for MCOF-Ru and MCOF-Ru/Re, respectively, which could be converted to -0.49 and -0.62 (V vs NHE). Accordingly, the conduction band (E_{CB}) of MCOF-Ru and MCOF-Ru/Re were estimated to be -0.59 and -0.72 (V vs NHE), respectively.

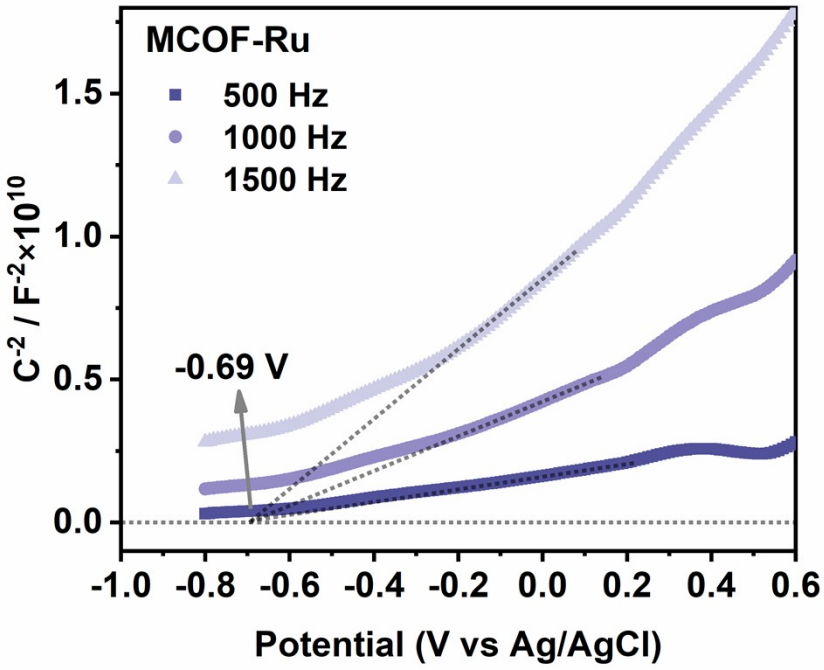

Figure S32. Mott-Schottky measurement of MCOF-Ru.

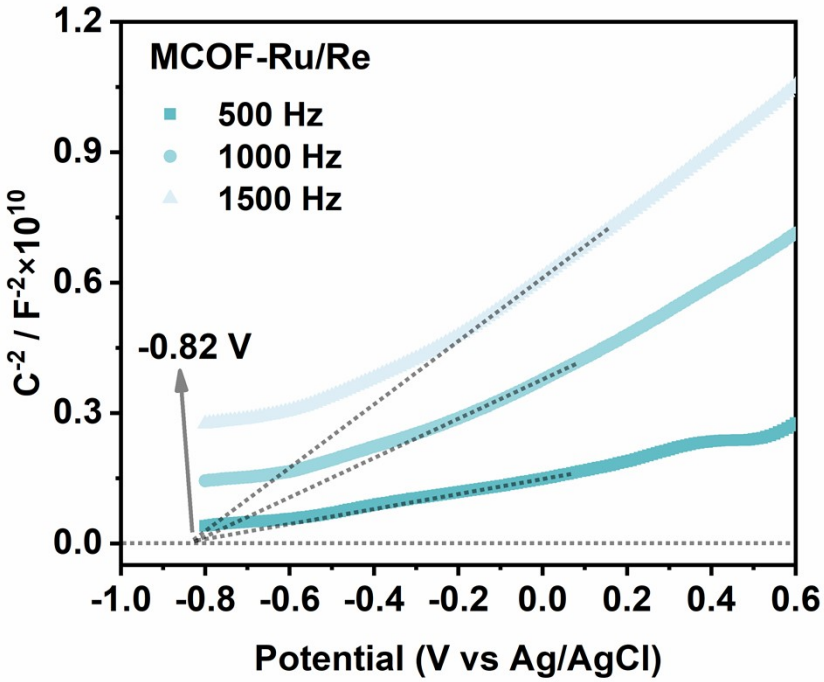

Figure S33. Mott-Schottky measurement of MCOF-Ru/Re.

4.3 CO_2 uptake of MCOFs

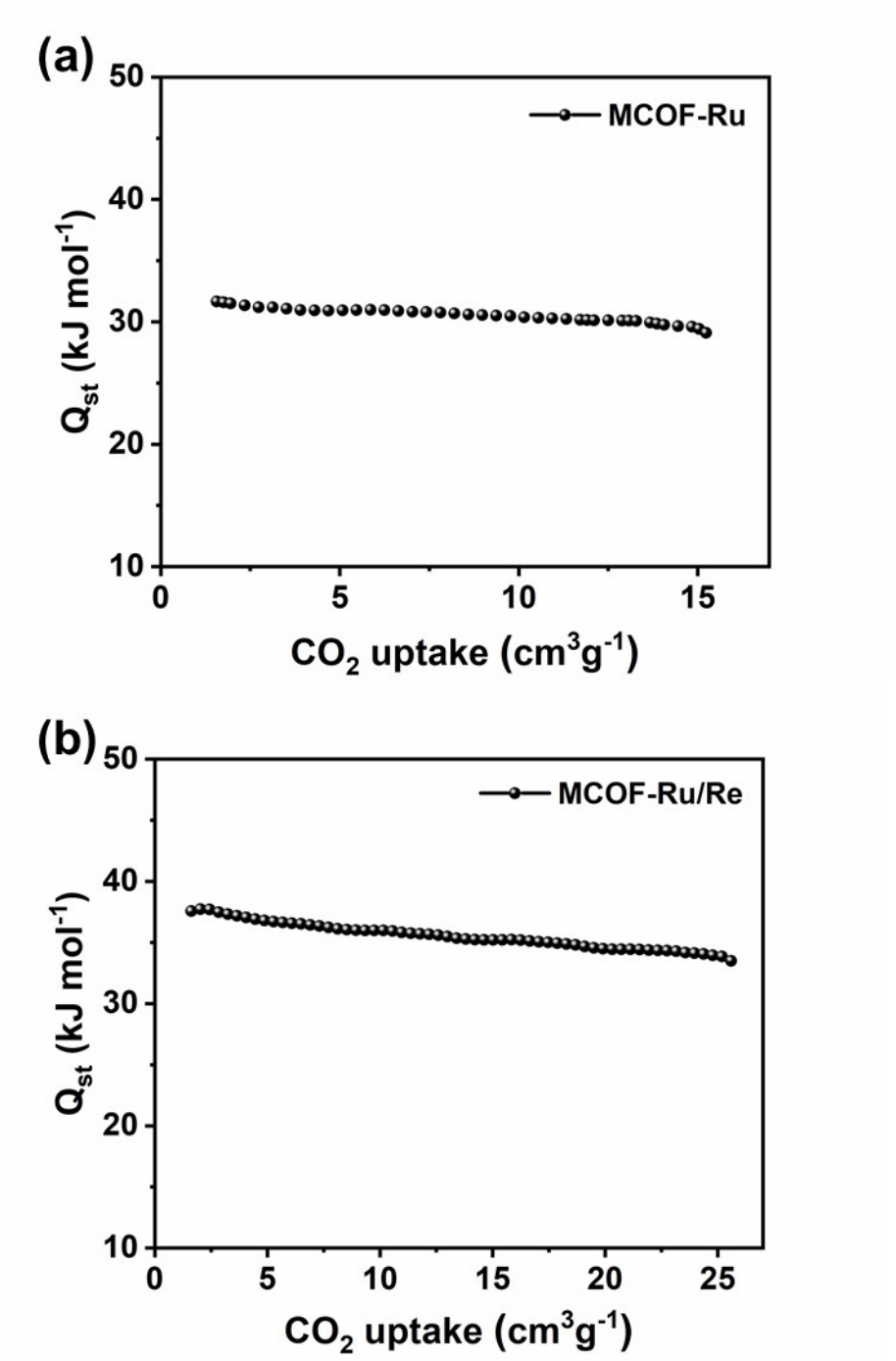

Figure. S34 The heat of adsorption (Q_{st}) of CO_2 for (a) MCOF-Ru and (b) MCOF-Ru/Re.

4.4 Apparent quantum efficiency measurement

The apparent quantum efficiency (AQE) for photocatalytic CO_2 reduction was evaluated using monochromatic lights, where the Xe lamp was equipped with 420 nm band-pass filter. The average intensity of irradiation was measured by using an optical photodiode power meter (ILT 950 Spectroradiometer). The sample was irradiated for 1 hour and the photocatalytic products were collected to analyze the yield. The irradiation area was controlled as 7.06 cm^2 (3.14 × 1.25^2 cm^2). The number of incident photons (N_p) is calculated by the following equation:

$$N_p = \frac{S \times P \times t \times \lambda}{h \times c}$$

Then, the AQE is calculated by following the equation:

$$AQE = \frac{2 \times N_e}{N_p} \times 100\% = \frac{2 \times M \times N_A \times h \times c}{S \times P \times t \times \lambda} \times 100\%$$

Where, N_e is the number of generated electrons, N_p is the number of incident photons, M is the amount of CO (mol), N_A is Avogadro constant (6.022×10^{23} mol^{-1}), h is the Planck constant (6.626×10^{-34} J·s), c is the speed of light (3×10^8 m s^{-1}), S is the irradiation area (cm^2), P is the intensity of irradiation light (W cm^{-2}), t is the photoreaction time (s), λ is the wavelength of the incident monochromatic light (m).

4.5 Photocatalytic CO_2 reduction

The photocatalytic performance was carried out in a 25 mL quartz reaction vessel with sealing components. Typically, 2.0 mg of photocatalyst, 0.4 mL TEOA and 0.02 M of BIH were suspended in 10 mL MeCN with sonication for 20 min to get a uniformly dispersed suspension. Then, the mixture was purged with high purity CO_2 for 20 min to remove air, ensuring that the final reactor was filled with CO_2. Subsequently, the suspension was irradiated under a 300 W Xe lamp (Perfect Light PLS-SXE 300) with a 420 nm cutoff filter to imitate visible light irradiation (420 nm ≤ λ ≤ 780 nm). The mixture was kept stirring during photocatalytic reaction. The temperature was maintained at 25 ºC using a condenser. After a certain period of irradiation, the gas products in the headspace (0.3 mL) of the reactor were detected by a gas chromatographer equipped with thermal conductivity detector (TCD) and flame ionization detector (FID). The carbon source for the isotope-labeling measurements was $^{13}CO_2$ gas instead of $^{12}CO_2$ gas. The gas product was identified by gas chromatography-mass spectrometry. For the blank experiments, control conditions were applied respectively on the basis of the above standard photocatalytic steps. The following control conditions were introduced, (1) Ar instead of CO_2 atmosphere, (2) No photocatalyst, (3) In dark condition, (4)

physical mixture of MCOF-Ru and $Re(CO)_5Cl$. For the recyclability test, the catalysts were separated from the reaction mixtures by centrifugation and washed with DMF, water, and THF for several times. After dried at 90 °C in a vacuum oven, the catalysts were reused for the next run under the reaction conditions.

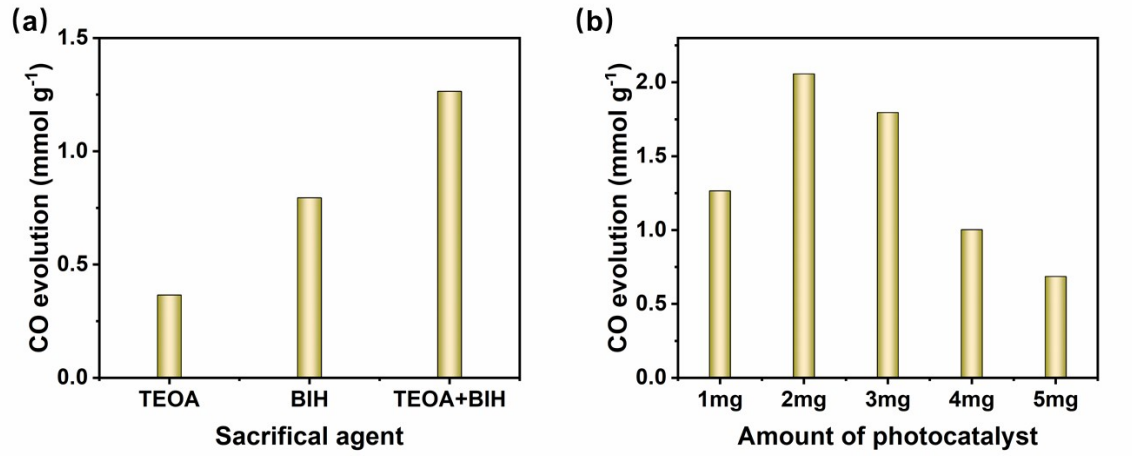

Figure S35. (a) The optimization of sacrificial agent within 1 h reaction (1 mg MCOF-Ru/Re in 10 mL MeCN with 0.4 mL of TEOA, 0.02 M of BIH, 0.4 mL of TEOA and 0.02 M of BIH, respectively). (b) The optimization of MCOF-Ru/Re photocatalyst amount within 1 h reaction (varying MCOF-Ru/Re concentrations in 10 mL MeCN with 0.4 mL of TEOA and 0.02 M of BIH).

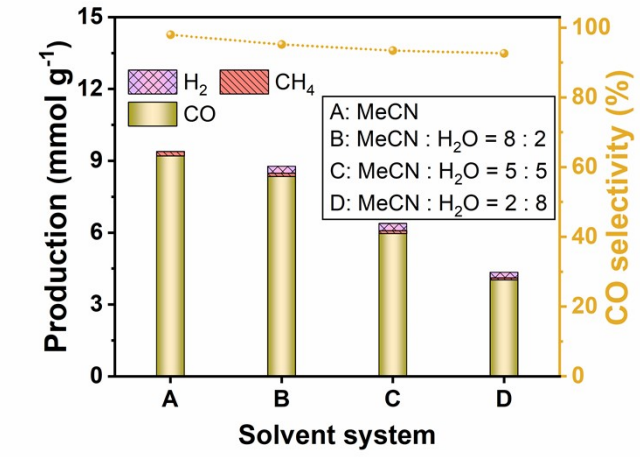

Figure S36. The comparison of solvent system to the influence on CO selectivity in photocatalytic reaction (2 mg MCOF-Ru/Re in 10 mL solvent with 0.4 mL of TEOA and 0.02 M of BIH in 5 h reaction).

For the evaluation of photocatalytic CO_2 performance, the choose of sacrificial electron donor is very important. Specifically, the sacrificial electron donor triethanolamine (TEOA)

and 1,3-dimethyl-2-phenyl-2,3-dihydro-1H-benzo[d]imidazole (BIH) have been widely used in photocatalytic systems for CO_2 reduction. And the optimization of sacrificial agent for achieving better photocatalytic performance was carried out. The combination of TEOA and BIH in our catalytic system showed a significant improvement in the efficiency of photocatalyst for CO_2 reduction. As previously reported (*J. Am. Chem. Soc. 2016, 138, 13818-13821; J. Catal., 2013, 304, 22-28.*), the BIH firstly donated one-electron to the photocatalyst and formed the one-electron oxidized form of $BIH^{+\bullet}$. Then, the TEOA functioned as a base for deprotonation of $BIH^{+\bullet}$, forming the intermediate state of $BI^{\bullet}$, thereby suppressing the back electron transfer from the photocatalyst to $BIH^{+\bullet}$. Furthermore, the $BI^{\bullet}$ intermediate was reported to have strong reducing power and to further donate one-electron to photocatalyst. Therefore, the combination of these two different sacrificial reagents accelerates the photocatalytic CO_2 reduction.

Additionally, the optimization of the photocatalyst amount was undertaken. In our system, the most effective concentration for photocatalytic CO_2 reduction was determined to be 0.2 mg/mL. Beyond this concentration, an increase in the catalyst amount led to a decline in catalytic performance. One reason for this phenomenon is that a smaller amount of catalysts is usually better dispersed in the solution, leading to a greater affective surface area. Besides, this decrease could also be attributed to the heightened shading effect resulting from an excess of catalyst content.

The photocatalytic experiment in the presence of water was also carried out. Our results revealed that as the content of H_2O in the solvent system increased, the overall CO_2 photocatalytic activity decreased. This decrease can be attributed to the inherent low solubility of CO_2 in aqueous solution (*Chem. Soc. Rev., 2023, 52, 4343-4380; iScience, 2019, 19, 135-160.*). Besides, the CO selectivity showed a slight decrease from 97.7% (MeCN) to 95.2% (MeCN: H_2O = 8:2), further decreasing to 92.6% (MeCN: H_2O = 2:8). This decrease is likely due to water competing with CO_2 photoreduction.

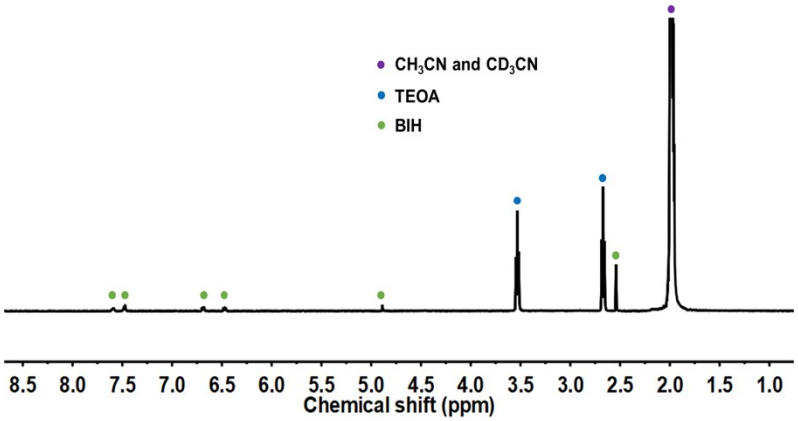

Figure S37. A representative ^{1}H NMR spectrum of liquid phase generated from CO_2 reduction catalyzed by MCOF-Ru/Re. CD_3CN was used as internal references.

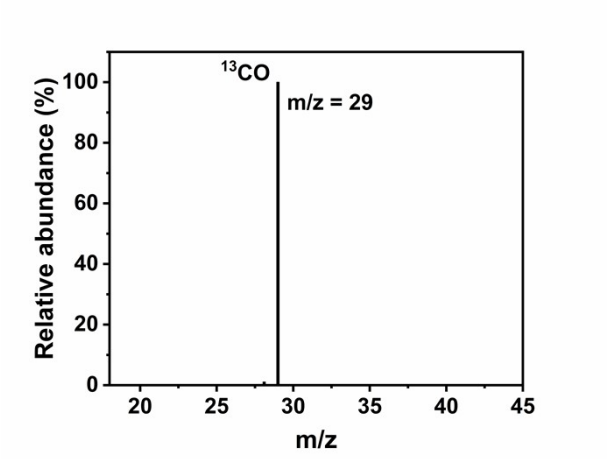

Figure S38. Mass spectrum of ^{13}CO produced from the photocatalytic reduction of $^{13}CO_2$ atmosphere after 10 h photoirradiation.

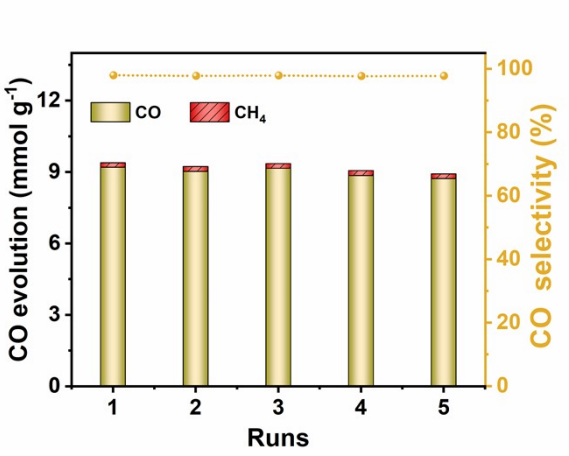

Figure S39. The recyclability of photocatalytic CO_2RR for MCOF-Ru/Re.

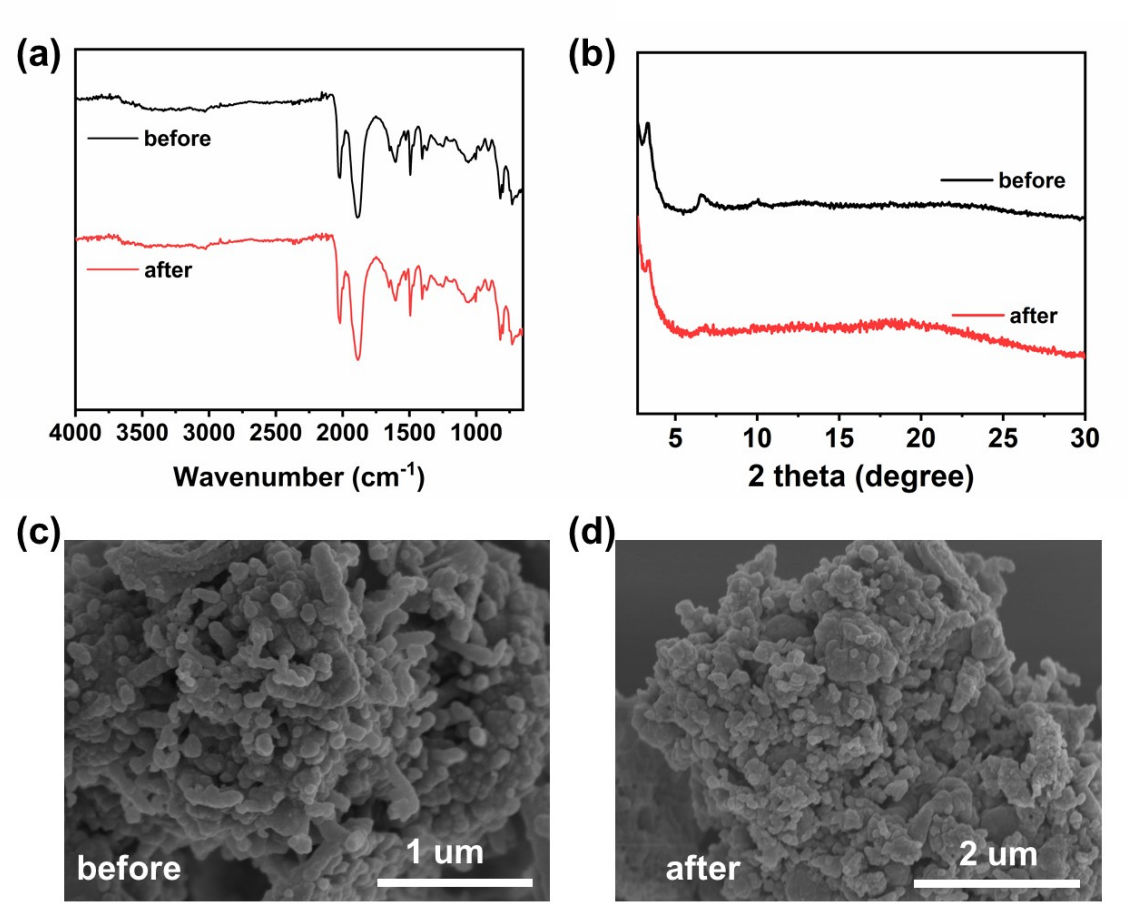

Figure. S40 (a) IR spectra, (b) PXRD patterns and (c-d) SEM images of MCOF-Ru/Re before and after 5 photocatalytic runs.

4.6 Comparison of photocatalytic CO_2 reduction activity

Table S2. Comparison of CO production with that catalyzed by other MCOFs and COFs based photocatalysts.

Entry	Photocatalyst amount	Photosensitizer $[Ru(bpy)_3]Cl_2$ amount	Photocatalyst	Irradiation condition	CO (umol g^{-1} h^{-1})	Selectivity (%)	[b] CO (umol g^{-1} h^{-1})	AQE (%)	Ref.
1	10 mg	60 mg	Co-TAPT-COF-2	λ > 420 nm	3500	42.5	500	/	13
2	10 mg	60 mg	Co-TAPT-COF-1	λ > 420 nm	8390	42.6	1198	0.006	
3	5 mg	10 mg	Fe SAS/Tr-COF	λ > 420 nm	980.3	96.4	327	3.17 (420 nm)	14
4	5 mg	10 mg	Tr-COF	λ > 420 nm	36.5	62.1	12	0.54 (420 nm)	
5	1 mg	10 mg	TP-COF	λ > 420 nm	960	74.5	87	/	15
6	1 mg	10 mg	2,3-DHTA-COF	λ > 420 nm	760	76.7	69	/	
7	1 mg	10 mg	Co-2,3-DHTA-COF	λ > 420 nm	18000	95.7	1636	0.47 (450 nm)	
8	20 mg	22.5 mg	DQTP COF-Co	λ > 420 nm	1020	90	480	/	16
9 [a]	1 mg	14.5 mg	Re-Bpy-sp2c-COF	λ > 420 nm	1400	86	90	0.5 (420 nm)	17
10	10 mg	6.5 mg	Ni-TpBpy	λ > 420 nm	966	96	585	0.3 (420 nm)	18
11	1 mg	4.3 mg	CoNi-COF-3	λ > 420 nm	2567	92.2	484	2.95 (450 nm)	19
12	2 mg	10 mg	CoPor-DPP-COF	λ > 420 nm	10200	82	1700	/	20
13	2 mg	10 mg	Co-PyPor-COF	λ > 420 nm	9645	96.7	1607.5	/	21
14	5 mg	19 mg	COF-367-Co NSs	λ > 420 nm	10162	78	2117	/	22
15 [a]	1 mg	1.12 mg	Co-FPy-CON	λ > 420 nm	1681	76	793	6.6 (420 nm)	23

16	5 mg	30 mg	H-COF-Ni	λ > 420 nm	2847	96	406	0.9 (420 nm)	24
17	5 mg	20 mg	Ni-PCD@TD-COF	λ > 420 nm	478	98	95.6	0.31 (420 nm)	25
18	2 mg	10 mg	ETTA-Bpy-COF-Co	λ > 420 nm	9398.14	92.73	1566	0.99 (420 nm)	26
19	5 mg	7 mg	Ni@TPHH-COF	λ > 420 nm	3250	95	1354	3.96 (420 nm)	27
20	20 mg	/	C_3N_4 (NH)/COF	λ > 400 nm	562	90	562	/	28
21	5 mg	/	CdS@COF	λ > 420 nm	507	72	507	0.21 (420 nm)	29
22	0.9 mg	/	Re-COF	λ > 420 nm	750	98	750	/	30
23	10 mg	/	LaNi-Phen/COF-5	λ > 380 nm	608	98.2	608	/	31
24	10 mg	/	Ni-Phen/COF-5	λ > 380 nm	224.4	91.2	224.4	/	
25	10 mg	/	La-Phen/COF-5	λ > 380 nm	195.4	95.9	195.4	/	
26	5 mg	/	pNJU-319Fe	λ > 420 nm	68.8	90	68.8	/	32
27	5 mg	/	NJU-319Fe	λ > 420 nm	26.8	83	26.8	/	
28	10 mg	/	PI-COF-TT	λ >300 nm	483	93	483	0.55 (380 nm)	33
29	3 mg	/	1D PyTTACOF-Co	λ > 420 nm	125.4	71	125.4	0.04 (420 nm)	34
30	**2 mg**	**/**	**MCOF-Ru/Re**	**λ > 420 nm**	**1840**	**97.7**	**1840**	**1.16 (420 nm)**	**This work**

(a) Ir[dF(CF_3)-ppy]$_2$(dtbpy))PF_6 was used as photosensitizer. (b) The amounts of photosensitizers were considered for the calculation of catalytic performance (i.e., $g_{total} = g_{catalyst} + g_{photosensitizer}$).

TOF calculations

Turnover frequency (TOF) is defined as moles of produced product per mole of catalyst per h^{-1}. Herein, for the calculation of TOF, the catalyst amount is referred to the amount of Re(I) active site in MCOF-Ru/Re. For MCOF-Ru/Re, each unit cell contains four coordination sites for Re(I) on four 2,2'-bipyrimidine ligands. Taking into account that 56% of the available coordination sites on the 2,2'-bipyrimidine ligands were converted to Re(I) sites, the molecular formula of $[C_{328}H_{216}N_{48}Ru_4P_8F_{48}]$ $[Re(CO)_3Cl]_{2.24}$ was used.

$$TOF\ (h^{-1}) = \frac{moles\ of\ CO\ evolution}{(moles\ of\ active\ Re(I)\ sites) \times time\ (h)}$$

Table S3. The comparison of TOF for CO evolution of the as-synthesized MCOF with other Ru-based and Ir-based system.

Photocatalyst	Type	Time (h)	TOF (h^{-1})	Ref.
RuC2PhC2Re	homogeneous	60	64.67	35
RuC2Re		60	45	
(RuRe+Ru)/Al_2O_3		60	48	36
RuDAC/ReDAC		4	25	37
RuBPY/ReDAC		4	7	
Ru-PSO_2P-Re		16	1.94	38
[a] $[Ir1^+][Ir2^-]$/Re(dtb)$(CO)_3$Cl		3	16.67	39
[b] (Ir[dF(CF_3)ppy]$_2$(dtbpy))PF_6/Co-FPy-CON	heterogeneous	6	4.68	40
Re-Bpy-sp2c-COF		17.5	1.07	41
MCOF-Ru/Re		**5**	**5.81**	**This work**

The TOF of MCOF-Ru/Re was estimated to be 5.81 h^{-1}. This value is comparable to that of some homogeneous molecular Ru/Re photocatalysts, such as RuBPY/ReDAC (7 h^{-1}), Ru-PSO_2P-Re (1.94 h^{-1}). Besides, our MCOF-Ru/Re showed a higher TOF compared to similar heterogeneous COF-based system, such as Re-Bpy-sp2c-COF (1.07 h^{-1}), (Ir[dF(CF_3)ppy]$_2$(dtbpy))PF_6/Co-FPy-CON (4.68 h^{-1}).

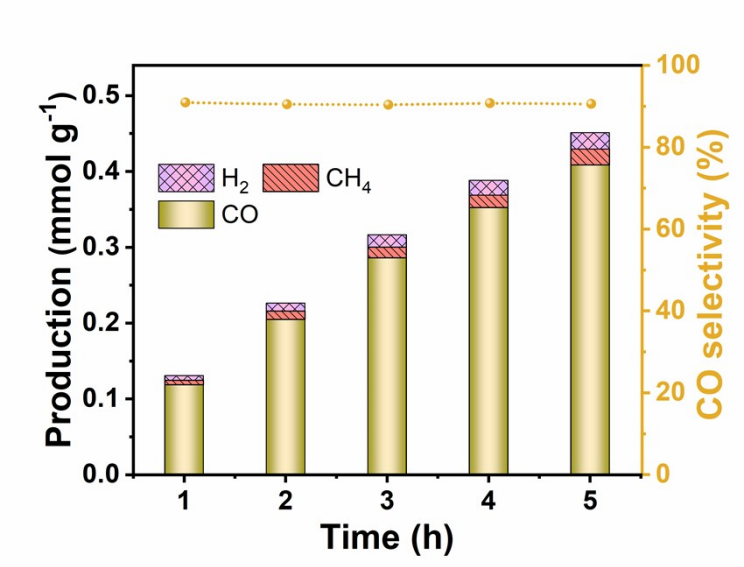

Figure. S41 The time-dependent photocatalytic CO_2 reduction in pure water condition.

Table S4. Comparison of photocatalytic CO_2 reduction in pure water condition with that by other COF-based photocatalysts.

Entry	Photocatalyst	Irradiation condition	CO (umol g^{-1} h^{-1})	Selectivity (%)	Ref.
1	TTCOF-Zn	λ > 420 nm	2.06	100	42
2	TAPBB-COF	λ > 200 nm	24.6	95.60	43
3	CT-COF	λ > 420 nm	102.7	98	
4	TFPB-COF	320-780	109.8	/	44
5	BTE-TBD-COF	320-780	382.03	/	
6	Mo-COF	λ > 420 nm	6.19	57.10	45
7	TCOF-MnMo6	λ > 400 nm	37.25	100	46
8	viCOF-bpy-Re	λ > 420 nm	190.6	100	47
9	COF-318-TiO_2	380-800	69.67	/	48
10	**MCOF-Ru/Re**	**λ > 420 nm**	**81.7**	**90.56**	**This work**

4.7 Charge separation and transfer dynamics

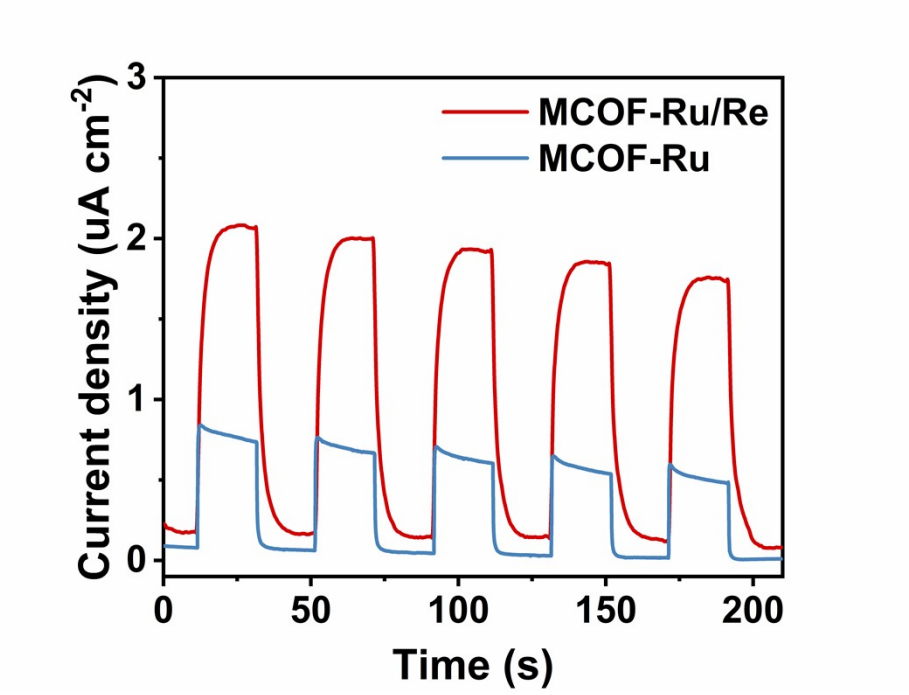

Figure. S42 The transient photocurrents responses for the MCOFs.

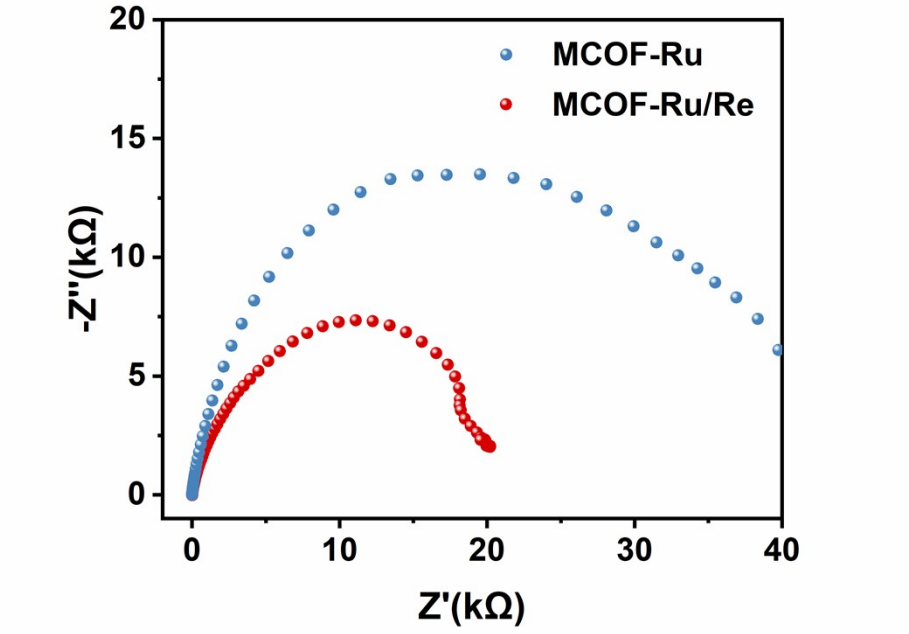

Figure. S43 The Nyquist plots for the MCOFs

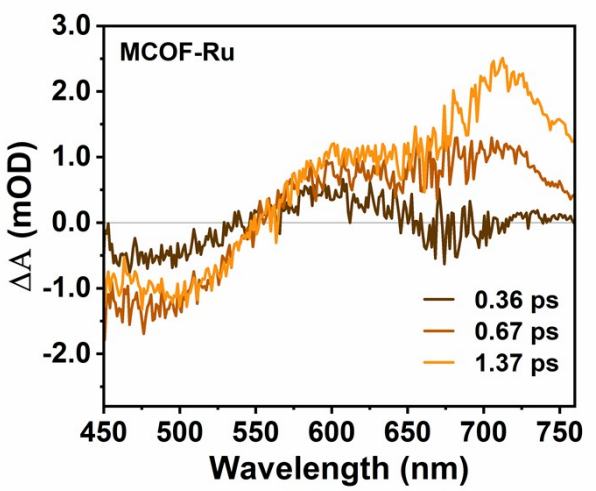

Figure. S44 Fs-TA spectra of MCOF-Ru in glycol, λ_{ex} = 350 nm.

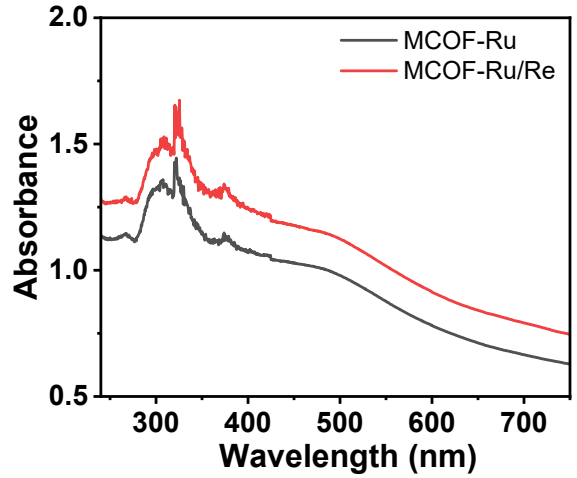

Figure. S45 UV-Vis spectra of MCOFs in glycol.

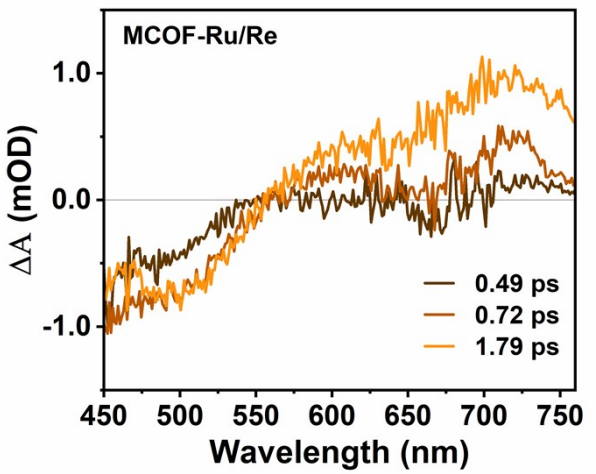

Figure. S46 Fs-TA spectra of MCOF-Ru/Re in glycol, λ_{ex} = 350 nm.

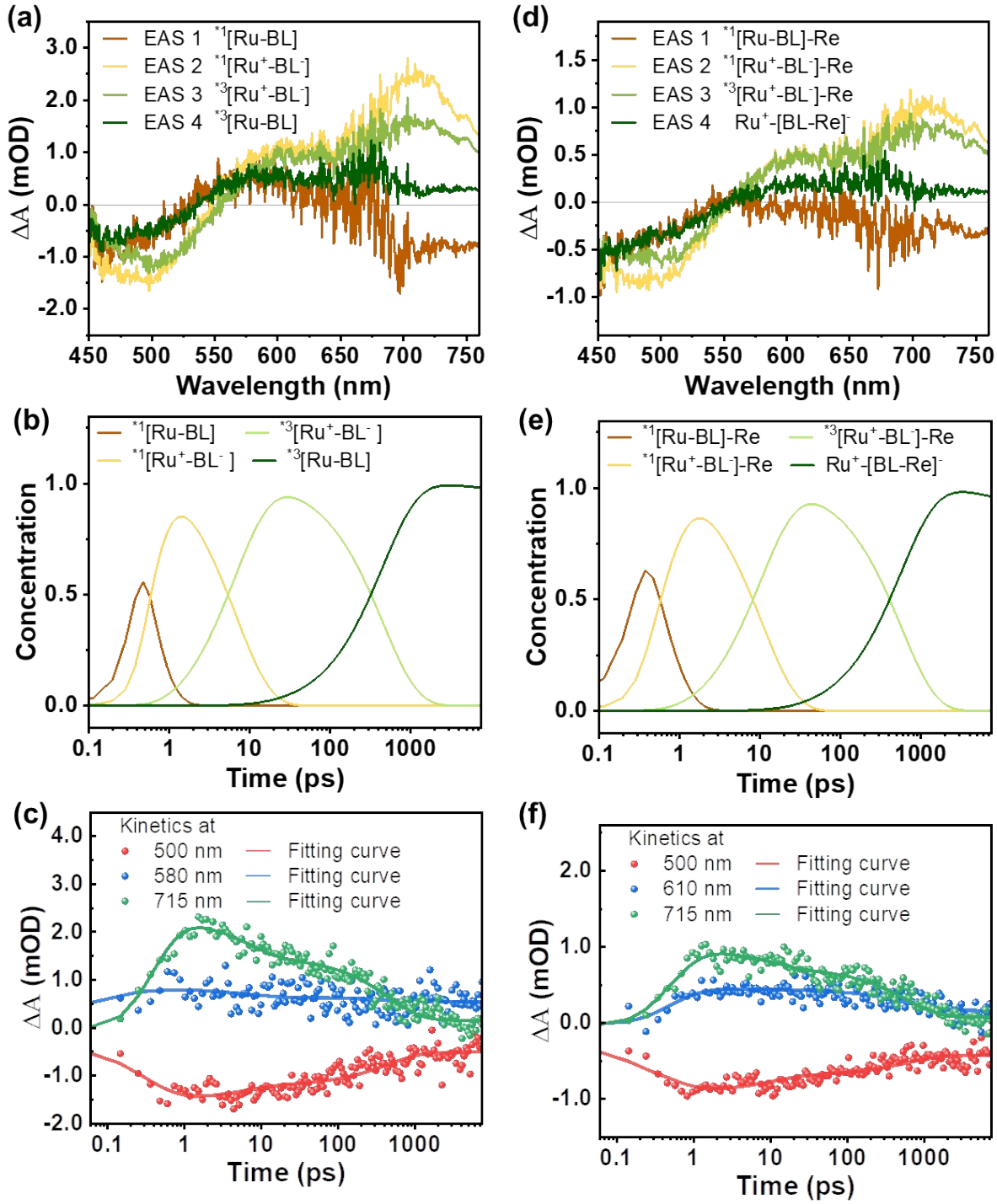

Figure. S47 Evolution-association dynamics spectra, Temporal concentrations of corresponding species and kinetics fitting of (a-c) MCOF-Ru with four lifetimes 0.34, 6.74, 451, and 3.48×105 ps, and (d-f) MCOF-Ru/Re with four lifetimes 0.47, 10.6, 568, and 1.69×105 ps.

4.8 Density functional theory (DFT) calculations

Density functional theory (DFT) computations was performed to further investigate the mechanism of photocatalytic reaction. Geometry optimizations and frequency calculations were conducted using the hybrid B3LYP exchange-correlation functional. The 6-31G(d) basis set for C, H, O, N and Cl atoms and LANL2DZ basis set for Ru and Re metal atoms were adopted. All calculations were carried out using Gaussian 09 software package.[48] The calculated model was constructed by first cutting a representing part from the simulated MCOFs structure, then the dangling bonds were saturated by hydrogens. The structures were fully optimized, following by the frequency calculation at the same level. The final electronic energies were further improved by single point calculations with an extended 6-31++G(d,p) basis set for the nonmetal atoms. Solvation effects were included by using SMD solvation model with acetonitrile as the solvent. Spin density surfaces of T1 states were generated by using Multiwfn and VMD programs.[49] Additionally, for our MCOF, the reaction center was Re unit. Therefore, in order to accelerate the computations, the Re part was used to study the CO_2RR towards CO, which, generally, was assumed to proceed through the following steps:

Step I: $* + CO_2 \rightarrow *CO_2$ Step II: $*CO_2 + H^+ + e^- \rightarrow *COOH$

Step III: $*COOH + H^+ + e^- \rightarrow *CO + H_2O$

Step IV: $*CO \rightarrow * + CO$, or $*CO + H^+ + e^- \rightarrow *CHO$

Where * represents the possible active site on computational model. The thermodynamic feasibility was evaluated by calculating the Gibbs free energy changes. And the associated free energies of species were calculated by the following expression:

$$G = E + ZPE - TS$$

Where E represents the total energy from DFT calculations. ZPE and TS are the correction from zero-point energy and entropic contributions, respectively. Besides, the free energy of $[H^+ + e^-]$ pair is approximately regarded as $1/2H_2$ in the calculation. Finally, the free energy change is described by the following expression:

$\Delta G_I = G_{*CO_2} - G_* - G_{CO_2}$ $\Delta G_{II} = G_{*COOH} - G_{*CO_2} - 0.5G_{H_2}$

$\Delta G_{III} = G_{*CO} + G_{H_2O} - G_{*COOH} - 0.5G_{H_2}$

$\Delta G_{IV} = G_* + G_{CO} - G_{*CO}$, or $\Delta G_{IV} = G_{*CHO} - G_{*CO} - 0.5G_{H_2}$

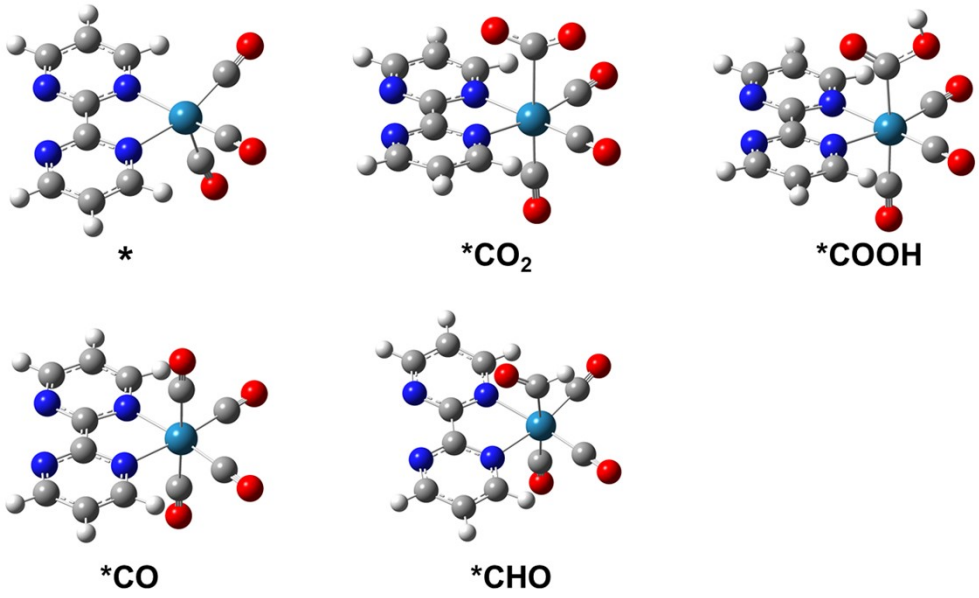

Figure S48. The DFT optimized structures for intermediate species.

4.9 Natural sunlight-driven CO_2 reduction

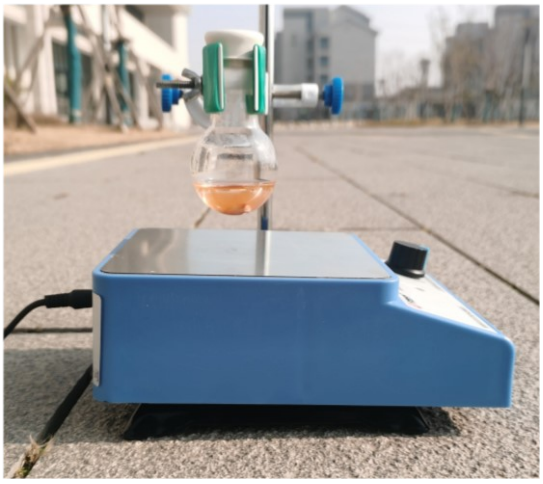

Figure S49. Experimental device and environment for natural sunlight-driven CO_2 reduction.

The natural sunlight-driven CO_2 reduction was carried out on the basis of the above standard photocatalytic steps. The quartz reaction vessel was placed outdoors of the campus at Jiangnan University. The photocatalytic reaction per day (from 9:00 am to 15:00 pm on Dec. 4th to Dec. 8th in 2023) was conducted for 5 consecutive days.

Section 5. Unit cell parameters and fractional atomic coordinates

Table S5. Unit cell parameters and fractional atomic coordinates for MCOF-Ru with **lvt** topology.

Space group: *Pnc*2			
Cell parameters: a = 30.15 Å, b = 45.72 Å, c = 30.16 Å, $\alpha = \beta = \gamma$ = 90°			
Atom	x(Å)	y(Å)	z(Å)
C1	1.73101	-1.74906	1.23765
C2	1.7756	-1.7527	1.24297
C3	1.87275	-1.88767	1.41247
C4	1.83501	-1.87164	1.42411
C5	1.82078	-1.84886	1.39734
C6	1.84385	-1.84178	1.35848
C7	1.88173	-1.85778	1.34714
C8	1.89613	-1.88051	1.37406
C9	1.94805	-1.62583	1.12885
C10	1.91132	-1.63596	1.10538
C11	1.88579	-1.65858	1.12228
C12	1.89654	-1.67133	1.16307
C13	1.93372	-1.66124	1.18638
C14	1.9594	-1.63869	1.16939
C15	1.62243	-1.59665	1.11616
C16	1.6546	-1.59431	1.14952
C17	1.67174	-1.61914	1.16944
C18	1.6571	-1.64671	1.15644
C19	1.62486	-1.64891	1.12308
C20	1.60766	-1.62404	1.10312
C21	1.56776	-1.87038	1.37589
C22	1.59791	-1.88029	1.34423
C23	1.62133	-1.86061	1.31809
C24	1.61485	-1.83068	1.3232
C25	1.58409	-1.82086	1.35467
C26	1.56069	-1.84051	1.38082
N27	-0.06298	0.01922	-0.48543
C28	-0.07661	0.04218	-0.50983
C29	-0.11881	0.05376	-0.50241
C30	-0.13508	0.07828	-0.52831
N31	-0.11246	0.08846	-0.56128
N32	-0.02782	-0.02647	-0.44057
C33	-0.06966	-0.01833	-0.42934
C34	-0.09272	-0.03396	-0.39699
C35	-0.07223	-0.05801	-0.37749
C36	-0.02956	-0.06624	-0.39067
C37	-0.0075	-0.04984	-0.42274
C38	-0.14588	0.04149	-0.46978
C39	-0.13097	0.0178	-0.44509
C40	-0.0887	0.00676	-0.45355
N41	0.02801	-0.10169	-0.38843
C42	-0.00833	-0.09176	-0.37137
C43	-0.38303	0.45451	-0.89529
N44	-0.3955	0.42843	-0.90506
N45	-0.54582	0.60898	-1.09652
C46	-0.5182	0.61616	-1.06557

N47	-0.54902	0.49968	-0.9707
N48	-0.48854	0.5448	-1.01666
C49	-0.40459	0.5317	-0.92831
C50	-0.56294	0.47237	-0.96073
C51	-0.56544	0.52358	-0.95044
C52	-0.5544	0.41911	-0.97983
C53	-0.54259	0.44814	-0.98587
C54	-0.59803	0.52037	-0.91783
C55	-0.46597	0.60202	-1.00608
C56	-0.38711	0.50743	-0.90684
C57	-0.50854	0.56478	-1.04272
C58	-0.49743	0.59402	-1.03788
N59	-0.45494	1.00292	-0.57308
N60	-1.0217	1.52599	-1.04264
C61	-1.17236	0.18169	-0.67057
C62	-1.13241	0.30615	-0.81767
C63	-1.32431	0.32703	-0.82257
C64	-1.35802	0.19023	-0.70209
C65	-1.29259	0.32948	-1.7888
C66	-1.27456	0.30481	-1.76924
C67	-1.28769	0.2772	-1.78338
C68	-1.31986	0.27459	-1.81654
C69	-1.33793	0.29933	-1.83609
C70	-1.20597	0.20036	-1.65594
C71	-1.22258	0.22183	-1.6838
C72	-1.20629	0.22478	-1.72704
C73	-1.17205	0.20662	-1.74148
C74	-1.15526	0.1852	-1.71347
C75	-1.32524	0.18052	-1.73155
C76	-1.29708	0.20023	-1.75241
C77	-1.30118	0.22997	-1.74395
C78	-1.33474	0.2398	-1.71571
C79	-1.36287	0.22009	-1.69492
C80	-1.16685	0.29397	-1.84273
C81	-1.1962	0.27429	-1.82353
C82	-1.19187	0.26672	-1.77877
C83	-1.15678	0.27823	-1.75403
C84	-1.12733	0.29779	-1.7733
C85	-1.58957	0.50605	-1.06946
C86	-1.61495	0.50792	-1.108
C87	-1.59338	0.50652	-1.14899
N88	-1.54857	0.50341	-1.15095
C89	-1.52443	0.50162	-1.11308
C90	-0.95712	0.44822	-1.03903
C91	-0.94514	0.43347	-1.07757
C92	-0.95554	0.44591	-1.11855
N93	-0.9769	0.47186	-1.12051
C94	-0.98828	0.48589	-1.08263
H95	1.81597	-1.87729	1.45556
H96	1.79018	-1.83583	1.40697
H97	1.90097	-1.85226	1.31577
H98	1.92706	-1.8933	1.36471
H99	1.90224	-1.62566	1.07228
H100	1.85593	-1.66684	1.10293

H101	1.94312	-1.67149	1.21942
H102	1.98962	-1.6307	1.18846
H103	1.66673	-1.57201	1.1603
H104	1.69787	-1.61715	1.19654
H105	1.61253	-1.67112	1.1121
H106	1.58147	-1.62605	1.07608
H107	1.60334	-1.90456	1.33978
H108	1.64595	-1.8688	1.29234
H109	1.57808	-1.79664	1.35902
H110	1.53576	-1.83232	1.40626
H111	-0.0538	0.05184	-0.53605
H112	-0.16823	0.08847	-0.51912
H113	-0.12755	-0.02705	-0.38694
H114	-0.09028	-0.07093	-0.35085
H115	0.02732	-0.0562	-0.43366
H116	-0.18024	0.05082	-0.46326
H117	-0.15318	0.00784	-0.41861
H118	-0.02369	-0.10292	-0.34139
H119	-0.35684	0.45818	-0.86867
H120	-0.50988	0.63995	-1.05971
H121	-0.39284	0.5545	-0.9198
H122	-0.5527	0.54597	-0.96003
H123	-0.5802	0.41302	-0.95389
H124	-0.45695	0.62582	-1.00162
H125	-0.36063	0.51024	-0.88026
H126	-0.53413	0.55769	-1.06829
H127	-1.28157	0.3519	-1.7774
H128	-1.24904	0.30704	-1.74162
H129	-1.33138	0.25222	-1.82766
H130	-1.36395	0.29712	-1.86325
H131	-1.2197	0.19787	-1.62097
H132	-1.24956	0.23711	-1.67146
H133	-1.1578	0.20929	-1.77621
H134	-1.12747	0.17041	-1.72539
H135	-1.32172	0.15634	-1.73837
H136	-1.27066	0.19216	-1.77641
H137	-1.33915	0.26401	-1.70966
H138	-1.39009	0.2282	-1.67186
H139	-1.17074	0.30026	-1.87904
H140	-1.22383	0.26431	-1.84425
H141	-1.15219	0.27161	-1.71794
H142	-1.09888	0.3071	-1.75296
H143	-1.60631	0.50716	-1.03566
H144	-1.65244	0.51052	-1.10566
H145	-1.61334	0.50798	-1.18096
H146	-0.94907	0.43855	-1.00523
H147	-0.92727	0.41176	-1.07524
H148	-0.94612	0.43431	-1.15053
Ru149	0	0	-0.48969
Ru150	-0.5	0.5	-1.02012

Table S6. Unit cell parameters and fractional atomic coordinates for MCOF-Ru/Re with **lvt** topology.

Space group: *P*1			
Cell parameters: a = 30.10 Å, b = 46.02 Å, c = 30.20 Å, α = 89.0°, $\beta = \gamma$ = 90°			
Atom	x(Å)	y(Å)	z(Å)
C1	0.73123	0.25675	0.24985
C2	0.77358	0.25362	0.25373
C3	0.87221	0.11199	0.40968
C4	0.83651	0.12721	0.42373
C5	0.82196	0.15108	0.39932
C6	0.84267	0.16013	0.36041
C7	0.87846	0.14488	0.34661
C8	0.89317	0.12107	0.37117
C9	0.9379	0.37815	0.13018
C10	0.90127	0.3693	0.10873
C11	0.87592	0.34782	0.12768
C12	0.88671	0.33491	0.16858
C13	0.92362	0.3438	0.18996
C14	0.9491	0.3652	0.17092
C15	0.62092	0.40665	0.12336
C16	0.65141	0.41021	0.15662
C17	0.66889	0.3859	0.17758
C18	0.65627	0.3576	0.16577
C19	0.62573	0.35421	0.1325
C20	0.60821	0.37853	0.11151
C21	0.57636	0.1312	0.38358
C22	0.60564	0.12182	0.35206
C23	0.62879	0.14213	0.32754
C24	0.62296	0.17219	0.33412
C25	0.59325	0.18147	0.36552
C26	0.57014	0.16122	0.39002
N27	0.93913	0.01698	0.50689
C28	0.92474	0.04006	0.48309
C29	0.88421	0.05033	0.49094
C30	0.86731	0.07536	0.4665
N31	0.88766	0.08731	0.43386
N32	0.97616	0.97226	0.55221
C33	0.93596	0.97871	0.56319
C34	0.91577	0.96234	0.5962
C35	0.9375	0.93949	0.61682
C36	0.97866	0.93313	0.60426
C37	0.99778	0.95014	0.57132
C38	0.8596	0.03661	0.52338
C39	0.87529	0.0129	0.54751
C40	0.91588	0.00324	0.53871
N41	0.03749	0.90093	0.61077
C42	1.0013	0.9091	0.62566
C43	0.61281	0.45789	0.10989
N44	0.60256	0.43115	0.10111
N45	0.44579	0.60993	0.90938
C46	0.4729	0.61697	0.93969
N47	0.45371	0.49828	0.03248
N48	0.50756	0.54544	0.98624

C49	0.5879	0.53477	0.0751
C50	0.44229	0.47038	0.04229
C51	0.43683	0.52183	0.05319
C52	0.45429	0.41704	0.0235
C53	0.46331	0.44658	0.01711
C54	0.40628	0.51761	0.08606
C55	0.52436	0.60366	0.99776
C56	0.60581	0.51094	0.09706
C57	0.4866	0.56504	0.96071
C58	0.49478	0.59484	0.96609
N59	0.54338	0.00148	0.4295
N60	0.98134	0.52764	0.94946
C61	0.82631	0.18486	0.33385
C62	0.85882	0.31305	0.18951
C63	0.67513	0.33181	0.18778
C64	0.64894	0.19381	0.30995
C65	0.70561	0.33527	0.22107
C66	0.72383	0.31098	0.24137
C67	0.71212	0.28274	0.2285
C68	0.68122	0.27917	0.19585
C69	0.66299	0.30348	0.17558
C70	0.79488	0.20292	0.35123
C71	0.77819	0.22551	0.32562
C72	0.79221	0.23027	0.28185
C73	0.82428	0.21272	0.26475
C74	0.84115	0.1902	0.29051
C75	0.67989	0.18475	0.27975
C76	0.70607	0.20514	0.25924
C77	0.70188	0.23495	0.26879
C78	0.6703	0.24412	0.29792
C79	0.64415	0.22375	0.31835
C80	0.8249	0.30139	0.16577
C81	0.79753	0.28177	0.18618
C82	0.80324	0.27369	0.23094
C83	0.83762	0.28481	0.25439
C84	0.86511	0.30431	0.2339
C85	0.41436	0.5028	0.92982
C86	0.39279	0.50335	0.88875
C87	0.41579	0.50241	0.84857
N88	0.45816	0.50103	0.8507
C89	0.4777	0.50063	0.8904
C90	0.03702	0.44606	0.94965
C91	0.0466	0.43258	0.90857
C92	0.03691	0.44719	0.8684
N93	0.01854	0.4739	0.87056
C94	0.00971	0.48605	0.91026
Cl95	0.9352	0.47883	0.81864
C96	0.98165	0.52961	0.77061
O97	0.97119	0.54535	0.74392
C98	0.49749	0.45423	0.80038
C99	0.45521	0.50043	0.75047
O100	0.57064	0.4965	0.72398
O101	0.49591	0.42965	0.80084
C102	0.26871	0.74325	0.24987

C103	0.22636	0.74638	0.2538
C104	0.12775	0.888	0.40979
C105	0.16348	0.87279	0.42381
C106	0.17802	0.84894	0.39939
C107	0.15729	0.83988	0.36049
C108	0.12148	0.85512	0.34673
C109	0.10676	0.87892	0.3713
C110	0.06194	0.62176	0.13062
C111	0.09851	0.63065	0.10909
C112	0.12388	0.65213	0.12799
C113	0.11319	0.665	0.16895
C114	0.07634	0.65607	0.19043
C115	0.05084	0.63467	0.17142
C116	0.37887	0.59344	0.12298
C117	0.3484	0.58986	0.15625
C118	0.33094	0.61416	0.17728
C119	0.34357	0.64246	0.16552
C120	0.37408	0.64588	0.13224
C121	0.39158	0.62157	0.11118
C122	0.42356	0.86882	0.38357
C123	0.39428	0.87819	0.35205
C124	0.37114	0.85787	0.32753
C125	0.37698	0.82781	0.33411
C126	0.40669	0.81854	0.36552
C127	0.42979	0.8388	0.39001
N128	0.06084	0.98303	0.50693
C129	0.07524	0.95994	0.48314
C130	0.11577	0.94968	0.49102
C131	0.13266	0.92464	0.4666
N132	0.1123	0.91268	0.43397
N133	0.02379	0.02774	0.55224
C134	0.06398	0.02129	0.56324
C135	0.08416	0.03764	0.59627
C136	0.06242	0.06049	0.61689
C137	0.02127	0.06686	0.60431
C138	0.00216	0.04986	0.57135
C139	0.14036	0.9634	0.52346
C140	0.12466	0.98711	0.54758
C141	0.08408	0.99676	0.53877
N142	0.96244	0.09906	0.61081
C143	-0.00138	0.09089	0.6257
C144	0.38696	0.54221	0.10947
N145	0.39723	0.56895	0.10071
N146	0.5541	0.38998	0.90947
C147	0.52702	0.38295	0.93982
N148	0.54619	0.50174	0.03268
N149	0.4925	0.45452	0.98633
C150	0.4119	0.4653	0.07489
C151	0.55759	0.52965	0.04243
C152	0.56303	0.47821	0.05348
C153	0.54557	0.58297	0.0235
C154	0.53664	0.55342	0.0171
C155	0.5935	0.48248	0.08642
C156	0.47551	0.39632	0.99782

C157	0.39395	0.48916	0.09674
C158	0.51344	0.43489	0.96085
C159	0.50516	0.4051	0.96621
N160	0.45652	0.99855	0.42949
N161	0.01861	0.47276	0.94917
C162	0.17365	0.81516	0.33393
C163	0.14109	0.68688	0.18982
C164	0.32474	0.66824	0.18761
C165	0.35101	0.8062	0.30994
C166	0.29434	0.66475	0.22098
C167	0.27615	0.68903	0.24136
C168	0.28781	0.71728	0.22848
C169	0.31863	0.72087	0.19574
C170	0.33683	0.69658	0.17541
C171	0.20514	0.79713	0.35128
C172	0.22183	0.77453	0.32566
C173	0.20774	0.76974	0.28193
C174	0.17562	0.78726	0.26486
C175	0.15875	0.80978	0.29062
C176	0.32002	0.81526	0.2798
C177	0.29384	0.79487	0.25928
C178	0.29808	0.76506	0.26878
C179	0.3297	0.75588	0.29786
C180	0.35585	0.77626	0.31828
C181	0.17492	0.69858	0.16597
C182	0.20231	0.71823	0.18631
C183	0.19669	0.72629	0.23109
C184	0.16239	0.71513	0.25464
C185	0.13489	0.69561	0.23423
C186	0.58596	0.4967	0.93029
C187	0.60769	0.49569	0.88935
C188	0.58489	0.49646	0.84904
N189	0.54252	0.4982	0.85093
C190	0.52284	0.49913	0.89052
C191	0.96346	0.55451	0.95021
C192	0.95446	0.56838	0.90928
C193	0.96433	0.55401	0.86896
N194	0.98219	0.52713	0.87083
C195	0.99028	0.51454	0.91041
C196	0.05901	0.52027	0.82038
C197	0.02083	0.47245	0.77032
O198	0.09076	0.53092	0.8209
O199	0.03174	0.45698	0.74345
Cl200	0.5038	0.55004	0.79891
C201	0.54586	0.49747	0.7507
O202	0.43052	0.50105	0.72362
C203	0.73123	0.24314	0.7501
C204	0.77358	0.24627	0.75399
C205	0.87227	0.38797	0.90977
C206	0.83654	0.37277	0.92382
C207	0.82199	0.34889	0.89944
C208	0.84273	0.3398	0.86057
C209	0.87854	0.35502	0.84678
C210	0.89326	0.37884	0.8713

C211	0.93795	0.12175	0.63052
C212	0.90134	0.13061	0.60905
C213	0.87598	0.15208	0.628
C214	0.88673	0.16497	0.66893
C215	0.92362	0.15607	0.69034
C216	0.94911	0.13467	0.67129
C217	0.621	0.09331	0.62333
C218	0.65148	0.08973	0.65659
C219	0.66894	0.11403	0.67761
C220	0.65633	0.14233	0.66585
C221	0.62579	0.14575	0.63258
C222	0.60829	0.12144	0.61153
C223	0.57637	0.36872	0.88376
C224	0.60564	0.37809	0.85223
C225	0.6288	0.35777	0.82773
C226	0.623	0.32771	0.83436
C227	0.5933	0.31844	0.86579
C228	0.57018	0.33871	0.89025
N229	0.9391	0.4831	0.00683
C230	0.92473	0.46002	0.98302
C231	0.88421	0.44971	-0.0091
C232	0.86734	0.42466	0.96649
N233	0.88771	0.41267	0.93389
N234	0.97616	0.52773	0.05233
C235	0.93596	0.52127	0.06329
C236	0.91578	0.53759	0.09636
C237	0.93751	0.56044	0.11702
C238	0.97866	0.56683	0.10445
C239	0.99778	0.54985	0.07146
C240	0.85962	0.4634	0.02338
C241	0.8753	0.48709	0.04755
C242	0.91587	0.49678	0.03873
N243	0.03745	0.59905	0.11093
C244	1.00129	0.59086	0.12585
C245	0.61286	0.04208	0.60981
N246	0.60263	0.06883	0.60104
N247	0.4458	0.89007	0.40932
C248	0.47286	0.88302	0.43967
N249	0.45371	0.00176	0.53265
N250	0.50742	0.95454	0.48633
C251	0.58788	0.96521	0.57507
C252	0.44233	0.02967	0.54243
C253	0.43684	0.97823	0.5534
C254	0.45439	0.083	0.52354
C255	0.46334	0.05345	0.51717
C256	0.40634	0.98248	0.58631
C257	0.52432	0.89633	0.49775
C258	0.60583	0.98904	0.597
C259	0.48649	0.93495	0.46079
C260	0.49471	0.90515	0.46612
N261	0.5436	0.49843	0.92956
N262	0.98134	0.97258	0.44932
C263	0.82635	0.31506	0.83404
C264	0.85882	0.18682	0.68985

C265	0.67516	0.16811	0.68792
C266	0.64897	0.3061	0.8102
C267	0.7056	0.16463	0.72125
C268	0.72381	0.18891	0.7416
C269	0.71212	0.21716	0.72873
C270	0.68126	0.22074	0.69604
C271	0.66304	0.19644	0.67573
C272	0.79489	0.29702	0.85143
C273	0.77818	0.27442	0.82584
C274	0.79222	0.26964	0.78209
C275	0.8243	0.28716	0.76498
C276	0.8412	0.30969	0.79071
C277	0.67991	0.31515	0.77998
C278	0.70607	0.29476	0.75946
C279	0.70187	0.26495	0.76902
C280	0.67031	0.25578	0.79818
C281	0.64418	0.27616	0.81861
C282	0.82494	0.1985	0.66607
C283	0.79756	0.21813	0.68645
C284	0.80324	0.22619	0.73123
C285	0.83758	0.21505	0.75472
C286	0.86507	0.19555	0.73425
C287	0.41413	0.99705	0.43011
C288	0.39249	0.9963	0.3891
C289	0.41538	0.99713	0.34886
N290	0.45777	0.99864	0.35087
C291	0.47737	0.99929	0.39052
C292	0.03685	0.05421	0.44998
C293	0.04618	0.06789	0.40897
C294	0.03639	0.05341	0.36873
N295	0.01823	0.02663	0.37072
C296	0.00974	0.01426	0.41037
C297	0.94181	0.01959	0.31957
C298	0.98037	0.97148	0.27046
Cl299	0.91009	0.03028	0.31962
O300	0.96966	0.95589	0.24367
C301	0.49716	0.04504	0.29973
C302	0.45462	0.99858	0.25064
O303	0.57004	0.00215	0.22386
Cl304	0.49567	0.06962	0.29978
C305	0.26869	0.75683	0.75008
C306	0.22633	0.75371	0.754
C307	0.12776	0.6121	0.91002
C308	0.16349	0.62731	0.92403
C309	0.17802	0.65117	0.89962
C310	0.15727	0.66023	0.86074
C311	0.12145	0.645	0.84698
C312	0.10675	0.6212	0.87155
C313	0.06197	0.87823	0.6305
C314	0.09857	0.86936	0.60902
C315	0.12393	0.84789	0.62798
C316	0.11319	0.83501	0.66892
C317	0.07631	0.84394	0.69034
C318	0.05082	0.86533	0.67129

C319	0.37892	0.90665	0.62327
C320	0.34845	0.91023	0.65655
C321	0.33099	0.88593	0.67757
C322	0.34359	0.85763	0.66579
C323	0.3741	0.85421	0.63249
C324	0.3916	0.87853	0.61145
C325	0.42352	0.6312	0.88366
C326	0.39417	0.62184	0.85221
C327	0.37102	0.64217	0.82772
C328	0.37693	0.67223	0.83426
C329	0.40671	0.68148	0.8656
C330	0.42981	0.66121	0.89007
N331	0.06082	0.51703	0.00697
C332	0.07524	0.54014	0.98326
C333	0.11578	0.55038	-0.00885
C334	0.13269	0.57543	0.96678
N335	0.11232	0.58741	0.93418
N336	0.02377	0.47224	0.05209
C337	0.06397	0.47866	0.06311
C338	0.08414	0.46225	0.09608
C339	0.06239	0.43937	0.1166
C340	0.02124	0.43303	0.10401
C341	0.00213	0.45009	0.07111
C342	0.14037	0.5366	0.02355
C343	0.12466	0.51286	0.04759
C344	0.08406	0.50323	0.03874
N345	0.96238	0.40086	0.11048
C346	-0.00141	0.40899	0.12535
C347	0.38703	0.95789	0.60977
N348	0.39727	0.93114	0.60099
N349	0.55411	0.10995	0.40935
C350	0.52706	0.117	0.43971
N351	0.54617	0.99825	0.53265
N352	0.49246	0.04547	0.48635
C353	0.41199	0.03478	0.57507
C354	0.55755	0.97033	0.54242
C355	0.56305	0.02177	0.55343
C356	0.54553	0.91702	0.5235
C357	0.53656	0.94657	0.51714
C358	0.59354	0.0175	0.58634
C359	0.4756	0.10369	0.49781
C360	0.39405	0.01094	0.59698
C361	0.51341	0.06507	0.46081
C362	0.5052	0.09487	0.46616
N363	0.45674	0.50143	0.92932
N364	0.01866	0.02744	0.44935
C365	0.17362	0.68496	0.83416
C366	0.14109	0.81316	0.68985
C367	0.32475	0.83185	0.68786
C368	0.35096	0.69386	0.81011
C369	0.29433	0.83533	0.7212
C370	0.27612	0.81106	0.74156
C371	0.28779	0.78281	0.72869
C372	0.31863	0.77922	0.69599

C373	0.33686	0.80351	0.67567
C374	0.20511	0.70299	0.8515
C375	0.2218	0.72558	0.82587
C376	0.20771	0.73036	0.78214
C377	0.17558	0.71285	0.76509
C378	0.15871	0.69033	0.79086
C379	0.31995	0.68481	0.77999
C380	0.29378	0.7052	0.75949
C381	0.29805	0.73502	0.76898
C382	0.3297	0.74418	0.79804
C383	0.35584	0.72379	0.81844
C384	0.17496	0.80147	0.66607
C385	0.20234	0.78185	0.68646
C386	0.19667	0.77379	0.73124
C387	0.16233	0.78494	0.75472
C388	0.13484	0.80444	0.73426
C389	0.58576	0.00296	0.43012
C390	0.60741	0.00369	0.38912
C391	0.58451	0.00285	0.34887
N392	0.54213	0.00134	0.35088
C393	0.52252	0.00073	0.39052
C394	0.96314	0.94581	0.44992
C395	0.95382	0.93216	0.40891
C396	0.96362	0.94664	0.36867
N397	0.98178	0.97343	0.3707
C398	0.99027	0.98578	0.41035
C399	0.0582	0.98048	0.31956
C400	0.01966	0.02862	0.27049
O401	0.08994	0.9698	0.31962
O402	0.03037	0.04422	0.24372
C403	0.50275	0.95493	0.29972
C404	0.5453	0.00138	0.25064
O405	0.42989	0.99783	0.22385
O406	0.50424	0.93036	0.29979
Ru407	-0.00001	0	0.50273
Ru408	-0.00004	0.50008	0.00271
Ru409	0.50005	0.49998	0.98285
Re410	0.50045	0.49928	0.7997
Ru411	0.49994	0.00001	0.48291
Re412	0.49995	-0.00001	0.29975
Re413	0.0008	0.50077	0.81958
Re414	0.00001	0.00004	0.31958
H415	0.81938	0.12001	0.45522
H416	0.79301	0.16341	0.41094
H417	0.89578	0.15188	0.31513
H418	0.9224	0.10896	0.35983
H419	0.89211	0.37973	0.0756
H420	0.84617	0.34063	0.10992
H421	0.93303	0.33354	0.22314
H422	0.97907	0.37218	0.18848
H423	0.66188	0.43309	0.16648
H424	0.69363	0.38892	0.20455
H425	0.615	0.33144	0.12239
H426	0.58344	0.37549	0.08457

H427	0.61059	0.09748	0.34641
H428	0.65265	0.13434	0.30193
H429	0.5878	0.20576	0.37121
H430	0.54608	0.16902	0.4154
H431	0.94558	0.05088	0.45705
H432	0.83552	0.08431	0.47677
H433	0.88221	0.9677	0.60591
H434	0.9217	0.92598	0.64394
H435	1.03129	0.94533	0.56075
H436	0.82658	0.04474	0.53025
H437	0.85506	0.0018	0.57382
H438	0.98683	0.89758	0.65563
H439	0.63739	0.46272	0.13641
H440	0.48023	0.64091	0.94635
H441	0.59763	0.55806	0.08343
H442	0.44753	0.54474	0.04377
H443	0.43001	0.4102	0.04929
H444	0.53112	0.62788	1.00249
H445	0.63058	0.51463	0.12381
H446	0.46265	0.55718	0.93525
H447	0.71545	0.35818	0.23148
H448	0.74836	0.31407	0.26856
H449	0.67083	0.25634	0.18568
H450	0.638	0.30043	0.14888
H451	0.783	0.19901	0.38661
H452	0.75298	0.24025	0.34023
H453	0.83674	0.21677	0.22965
H454	0.8672	0.17599	0.27637
H455	0.68356	0.16054	0.27202
H456	0.73097	0.19757	0.23462
H457	0.66585	0.26834	0.30508
H458	0.61858	0.23135	0.34213
H459	0.8198	0.30806	0.12951
H460	0.77033	0.27221	0.16645
H461	0.8433	0.27796	0.29046
H462	0.89295	0.31326	0.25326
H463	0.39621	0.5035	0.96255
H464	0.35723	0.50455	0.8883
H465	0.3988	0.50281	0.81513
H466	0.04474	0.43456	0.98237
H467	0.06196	0.41015	0.90809
H468	0.0445	0.43659	0.83495
H469	0.18062	0.88	0.45529
H470	0.20699	0.83662	0.41098
H471	0.10414	0.8481	0.31526
H472	0.07752	0.89102	0.35998
H473	0.10759	0.62026	0.0759
H474	0.15357	0.65936	0.11015
H475	0.06701	0.66629	0.22365
H476	0.02093	0.62765	0.18906
H477	0.33791	0.56698	0.16607
H478	0.30621	0.61112	0.20427
H479	0.38482	0.66865	0.12215
H480	0.41633	0.62463	0.08423

H481	0.38931	0.90253	0.34638
H482	0.34727	0.86565	0.30192
H483	0.41215	0.79425	0.37122
H484	0.45385	0.83101	0.4154
H485	0.05441	0.94913	0.45709
H486	0.16447	0.9157	0.47685
H487	0.11771	0.03228	0.606
H488	0.07821	0.074	0.64402
H489	-0.03135	0.05466	0.56077
H490	0.17338	0.95526	0.53034
H491	0.14488	0.99821	0.5739
H492	0.01309	0.10241	0.65567
H493	0.36235	0.53738	0.13596
H494	0.5197	0.35902	0.94652
H495	0.40215	0.44202	0.08325
H496	0.55236	0.4553	0.0441
H497	0.56979	0.58984	0.04934
H498	0.46869	0.37211	1.00256
H499	0.36912	0.4855	0.12343
H500	0.53745	0.44272	0.93543
H501	0.28455	0.64184	0.23141
H502	0.25169	0.68592	0.26861
H503	0.32898	0.74371	0.18556
H504	0.36176	0.69966	0.14864
H505	0.21707	0.80107	0.38662
H506	0.24708	0.75982	0.34025
H507	0.16311	0.78318	0.22978
H508	0.13266	0.82396	0.27651
H509	0.31631	0.83947	0.27211
H510	0.26891	0.80245	0.23471
H511	0.3342	0.73166	0.30496
H512	0.38147	0.76864	0.34201
H513	0.17994	0.69191	0.1297
H514	0.22944	0.72781	0.1665
H515	0.15679	0.72198	0.29073
H516	0.10712	0.68662	0.25366
H517	0.60395	0.49607	0.96313
H518	0.64324	0.49428	0.88909
H519	0.602	0.49561	0.8157
H520	0.95573	0.56586	0.98306
H521	0.93941	0.59091	0.90904
H522	0.95732	0.56496	0.83562
H523	0.81939	0.38001	0.95528
H524	0.79302	0.33658	0.91106
H525	0.89589	0.34798	0.81534
H526	0.92251	0.39093	0.85996
H527	0.89222	0.12021	0.57589
H528	0.84625	0.15929	0.61021
H529	0.93299	0.1663	0.72354
H530	0.97906	0.12768	0.68888
H531	0.66196	0.06685	0.66641
H532	0.69368	0.11098	0.70458
H533	0.61506	0.16853	0.6225
H534	0.58352	0.1245	0.58459

H535	0.61058	0.40243	0.84653
H536	0.65266	0.36555	0.80211
H537	0.58787	0.29416	0.87153
H538	0.54614	0.33091	0.91566
H539	0.94556	0.44923	0.95694
H540	0.83553	0.41572	0.97675
H541	0.88223	0.53222	0.10607
H542	0.92172	0.57391	0.14418
H543	1.03128	0.55467	0.06089
H544	0.82661	0.45524	0.03026
H545	0.85508	0.49815	0.07391
H546	0.98684	0.60236	0.15585
H547	0.63744	0.03723	0.63633
H548	0.48018	0.85909	0.44634
H549	0.59759	0.94192	0.58341
H550	0.44751	0.95532	0.54399
H551	0.43016	0.08987	0.54937
H552	0.5311	0.87211	0.50246
H553	0.63061	0.98535	0.62373
H554	0.46252	0.94281	0.43535
H555	0.71542	0.14172	0.73166
H556	0.7483	0.18581	0.76881
H557	0.67089	0.24358	0.68587
H558	0.63809	0.19952	0.649
H559	0.78301	0.30096	0.8868
H560	0.75295	0.25971	0.84047
H561	0.83677	0.28309	0.72988
H562	0.86726	0.32388	0.77656
H563	0.68358	0.33936	0.77224
H564	0.73096	0.30232	0.73483
H565	0.66586	0.23156	0.80534
H566	0.61861	0.26856	0.84241
H567	0.81987	0.19184	0.6298
H568	0.77039	0.2277	0.6667
H569	0.84323	0.22189	0.7908
H570	0.89288	0.18657	0.75364
H571	0.39607	0.9964	0.46289
H572	0.35693	0.99505	0.38875
H573	0.39833	0.99652	0.31547
H574	0.04458	0.06563	0.48276
H575	0.06143	0.09035	0.40862
H576	0.04372	0.06418	0.33533
H577	0.18065	0.62009	0.9555
H578	0.20699	0.66349	0.9112
H579	0.1041	0.65202	0.81553
H580	0.0775	0.6091	0.86024
H581	0.10769	0.87975	0.57585
H582	0.15365	0.84067	0.61018
H583	0.06694	0.83371	0.72355
H584	0.02088	0.87234	0.68888
H585	0.33798	0.93311	0.66639
H586	0.30626	0.88897	0.70455
H587	0.38482	0.83144	0.6224
H588	0.41636	0.87547	0.5845

H589	0.38914	0.5975	0.84658
H590	0.3471	0.6344	0.80216
H591	0.41222	0.70577	0.87127
H592	0.45393	0.66899	0.91541
H593	0.05441	0.551	0.95725
H594	0.16449	0.58437	0.97704
H595	0.1177	0.46758	0.10581
H596	0.07818	0.42582	0.14368
H597	-0.03138	0.4453	0.06052
H598	0.1734	0.54472	0.03045
H599	0.14488	0.50171	0.07386
H600	0.01308	0.39742	0.15526
H601	0.36245	0.96273	0.63629
H602	0.51975	0.14094	0.44639
H603	0.40228	0.05807	0.58342
H604	0.55238	0.04469	0.54403
H605	0.56977	0.91015	0.54931
H606	0.46884	0.12791	0.50253
H607	0.36926	0.01462	0.62371
H608	0.53737	0.05721	0.43536
H609	0.28453	0.85825	0.73162
H610	0.25164	0.81416	0.76879
H611	0.32899	0.75638	0.68582
H612	0.3618	0.80043	0.64892
H613	0.21704	0.69906	0.88685
H614	0.24705	0.74029	0.84045
H615	0.16307	0.71692	0.73001
H616	0.13261	0.67615	0.77676
H617	0.31621	0.66059	0.77231
H618	0.26882	0.69764	0.73493
H619	0.33422	0.7684	0.80513
H620	0.38148	0.73139	0.84216
H621	0.18002	0.80813	0.6298
H622	0.22951	0.77227	0.6667
H623	0.15668	0.77809	0.79081
H624	0.10703	0.81342	0.75364
H625	0.60383	0.00361	0.4629
H626	0.64297	0.00493	0.38876
H627	0.60156	0.00344	0.31548
H628	0.95539	0.93439	0.4827
H629	0.93857	0.90969	0.40854
H630	0.9563	0.93588	0.33527

Section 6. References

(1) Liu, Y.; Diercks, C. S.; Ma, Y.; Lyu, H.; Zhu, C.; Alshmimri, S. A.; Alshihri, S.; Yaghi, O. M., *J. Am. Chem. Soc*. 2019, **141**, 677-683.

(2) Dolomanov. O. V., Bourhis. L. J., Gildea. R. J., Howard. J. A. K., Puschmann. H., *J. Appl. Cryst*. 2009, **42**, 339-341.

(3) Sheldrick. G. M., 2015, **A71**, 3-8.

(4) Sheldrick. G. M., *Acta Cryst.* 2015, **C71**, 3-8.

(5) Han, W. K.; Liu, Y.; Feng, J. D.; Yan, X.; Pang, H.; Gu, Z. G., *Chem. Sci*. 2023, **14**, 11768-11774.

(6) Qi, J.-Y.; Ji, J.-X.; Yueng, C.-H.; Kwong, H.-L.; Chan, A. S. C., *Tetrahedron Lett*. 2004, **45**, 7719-7721.

(7) Han, W. K.; Liu, Y.; Yan, X.; Jiang, Y.; Zhang, J.; Gu, Z. G., *Angew. Chem. Int. Ed*. 2022, **61**, e202208791.

(8) Johnson, E. M.; Haiges, R.; Marinescu, S. C., *ACS Appl. Mater. Interfaces* 2018, **10**, 37919-37927.

(9) Song, D.; Xu, W.; Li, J.; Zhao, J.; Shi, Q.; Li, F.; Sun, X.; Wang, N., *Chinese Journal of Catalysis* 2022, **43**, 2425-2433.

(10) http://rcsr.anu.edu.au/nets.

(11) Tauc, J.; Grigorovici, R.; Vancu, A., *physica status solidi (b)* 1966, **15**, 627-637.

(12) Yang, Y.; Liu, Z.; Ng, W. K.; Zhang, L.; Zhang, H.; Meng, X.; Bai, Y.; Xiao, S.; Zhang, T.; Hu, C.; Wong, K. S.; Yang, S., *Adv. Funct. Mater*. 2018, **29**, 1806506.

(13) Zhou, W.; Wang, X.; Zhao, W.; Lu, N.; Cong, D.; Li, Z.; Han, P.; Ren, G.; Sun, L.; Liu, C.; Deng, W. Q., *Nat. Commun*. 2023, **14**, 6971.

(14) Ran, L.; Li, Z.; Ran, B.; Cao, J.; Zhao, Y.; Shao, T.; Song, Y.; Leung, M. K. H.; Sun, L.; Hou, J., *J. Am. Chem. Soc*. 2022, **144**, 17097-17109.

(15) Zhang, Q.; Gao, S.; Guo, Y.; Wang, H.; Wei, J.; Su, X.; Zhang, H.; Liu, Z.; Wang, J., *Nat. Commun*. 2023, **14**, 1147.

(16) Lu, M.; Li, Q.; Liu, J.; Zhang, F. M.; Zhang, L.; Wang, J. L.; Kang, Z. H.; Lan, Y. Q., *Appl. Catal. B Environ* 2019, **254**, 624-633.

(17) Fu, Z.; Wang, X.; Gardner, A. M.; Wang, X.; Chong, S. Y.; Neri, G.; Cowan, A. J.; Liu, L.; Li, X.; Vogel, A.; Clowes, R.; Bilton, M.; Chen, L.; Sprick, R. S.; Cooper, A. I., *Chem. Sci*. 2020, **11**, 543-550.

(18) Zhong, W.; Sa, R.; Li, L.; He, Y.; Li, L.; Bi, J.; Zhuang, Z.; Yu, Y.; Zou, Z., *J. Am. Chem. Soc*. 2019, **141**, 7615-7621.

(19) Wang, J.; Zhu, W.; Meng, F.; Bai, G.; Zhang, Q.; Lan, X., *Acs. Catal*. 2023, **13**, 4316-4329.

(20) Wang, X.; Ding, X.; Wang, T.; Wang, K.; Jin, Y.; Han, Y.; Zhang, P.; Li, N.; Wang, H.; Jiang, J., *ACS Appl. Mater. Interfaces* 2022, **14**, 41122-41130.

(21) Luan, T. X.; Wang, J. R.; Li, K.; Li, H.; Nan, F.; Yu, W. W.; Li, P. Z., *Small* 2023, **19**, 2303324.

(22) Liu, W.; Li, X.; Wang, C.; Pan, H.; Liu, W.; Wang, K.; Zeng, Q.; Wang, R.; Jiang, J., *J. Am. Chem. Soc.* 2019, **141**, 17431-17440.

(23) Wang, X.; Fu, Z.; Zheng, L.; Zhao, C.; Wang, X.; Chong, S. Y.; McBride, F.; Raval, R.; Bilton, M.; Liu, L.; Wu, X.; Chen, L.; Sprick, R. S.; Cooper, A. I., *Chem. Mater*. 2020, **32**, 9107-9114.

(24) Yang, S.; Sa, R.; Zhong, H.; Lv, H.; Yuan, D.; Wang, R., *Adv. Funct. Mater.* 2022, **32**, 2110694.

(25) Zhong, H.; Sa, R.; Lv, H.; Yang, S.; Yuan, D.; Wang, X.; Wang, R., *Adv. Funct. Mater*. 2020, **30**, 2002654.

(26) Wang, Y.; Sun, T.; Zheng, T.; Ding, X.; Zhang, P.; Xu, Q.; Li, T.; Zhang, S.; Wang, K.; Xu, L.; Jiang, J., *ACS Materials Lett*. 2024, **6**, 140-152.

(27) Dong, M.; Zhou, J.; Zhong, J.; Li, H. T.; Sun, C. Y.; Han, Y. D.; Kou, J. N.; Kang, Z. H.; Wang, X. L.; Su, Z. M., *Adv. Funct. Mater*. 2022, **32**, 2110136.

(28) Wang, J.; Yu, Y.; Cui, J.; Li, X.; Zhang, Y.; Wang, C.; Yu, X.; Ye, J., *Appl. Catal. B Environ*. 2022, **301**, 120814.

(29) Zou, L.; Sa, R.; Zhong, H.; Lv, H.; Wang, X.; Wang, R., *Acs. Catal.* 2022, **12**, 3550-3557.

(30) Yang, S.; Hu, W.; Zhang, X.; He, P.; Pattengale, B.; Liu, C.; Cendejas, M.; Hermans, I.; Zhang, X.; Zhang, J.; Huang, J., *J. Am. Chem. Soc*. 2018, **140**, 14614-14618.

(31) Zhou, M.; Wang, Z.; Mei, A.; Yang, Z.; Chen, W.; Ou, S.; Wang, S.; Chen, K.; Reiss, P.; Qi, K.; Ma, J.; Liu, Y., *Nat. Commun*. 2023, **14**, 2473.

(32) Dong, P.; Xu, X.; Luo, R.; Yuan, S.; Zhou, J.; Lei, J., *J. Am. Chem. Soc.* 2023, **145**, 15473-15481.

(33) Chen, X.; Dang, Q.; Sa, R.; Li, L.; Li, L.; Bi, J.; Zhang, Z.; Long, J.; Yu, Y.; Zou, Z., *Chem. Sci*. 2020, **11**, 6915-6922.

(34) Zou, L.; Chen, Z. A.; Si, D. H.; Yang, S. L.; Gao, W. Q.; Wang, K.; Huang, Y. B.; Cao, R., *Angew. Chem. Int. Ed*. 2023, **62**, e202309820.

(35) K. Kamogawa, A. Santoro, A. M. Cancelliere, Y. Shimoda, K. Miyata, K. Onda, F. Puntoriero, S. Campagna, Y. Tamaki and O. Ishitani, *ACS. Catal*., 2023, **13**, 9025-9032.

(36) D. Saito, Y. Yamazaki, Y. Tamaki and O. Ishitani, *J. Am. Chem. Soc*. 2020, **142**, 19249-19258.

(37) P. L. Cheung, S. C. Kapper, T. Zeng, M. E. Thompson and C. P. Kubiak, *J. Am. Chem. Soc.*, 2019, **141**, 14961-14965.

(38) C. M. Brown, T. Auvray, E. E. DeLuca, M. B. Ezhova, G. S. Hanan and M. O. Wolf, *Chem. Commun*., 2020, **56**, 10750-10753.

(39) S. Y. Takizawa, T. Okuyama, S. Yamazaki, K. I. Sato, H. Masai, T. Iwai, S. Murata and J. Terao, *J. Am. Chem. Soc.*, 2023, **145**, 15049-15053.

(40) X. Wang, Z. Fu, L. Zheng, C. Zhao, X. Wang, S. Y. Chong, F. McBride, R. Raval, M. Bilton, L. Liu, X. Wu, L. Chen, R. S. Sprick and A. I. Cooper, *Chem. Mater*. 2020, **32**, 9107-9114.

(41) Z. Fu, X. Wang, A. M. Gardner, X. Wang, S. Y. Chong, G. Neri, A. J. Cowan, L. Liu, X. Li, A. Vogel, R. Clowes, M. Bilton, L. Chen, R. S. Sprick and A. I. Cooper, *Chem. Sci*., 2020, **11**, 543-550.

(42) M. Lu, J. Liu, Q. Li, M. Zhang, M. Liu, J. L. Wang, D. Q. Yuan and Y. Q. Lan, *Angew. Chem. Int. Ed.*, 2019, **58**, 12392-12397.

(43) K. Lei, D. Wang, L. Ye, M. Kou, Y. Deng, Z. Ma, L. Wang and Y. Kong, *ChemSusChem*, 2020, **13**, 1725-1729.

(44) L. Yang, W. Yan, N. Yang, G. Wang, Y. Bi, C. Tian, H. Liu and X. Zhu, *Small*, 2023, **19**, e2208118.

(45) M. Kou, W. Liu, Y. Wang, J. Huang, Y. Chen, Y. Zhou, Y. Chen, M. Ma, K. Lei, H. Xie, P. K. Wong and L. Ye, *Appl. Catal. B Environ*., 2021, **291**, 120146.

(46) M. Lu, M. Zhang, J. Liu, T. Y. Yu, J. N. Chang, L. J. Shang, S. L. Li and Y. Q. Lan, *J. Am. Chem. Soc.*, 2022, **144**, 1861-1871.

(47) Y. Z. Cheng, W. Ji, P. Y. Hao, X. H. Qi, X. Wu, X. M. Dou, X. Y. Bian, D. Jiang, F. T. Li, X. F. Liu, D. H. Yang, X. Ding and B. H. Han, *Angew. Chem. Int. Ed*., 2023, **62**, e202308523.

(48) M. Zhang, M. Lu, Z. L. Lang, J. Liu, M. Liu, J. N. Chang, L. Y. Li, L. J. Shang, M. Wang, S. L. Li and Y. Q. Lan, *Angew. Chem. Int. Ed.*, 2020, **59**, 6500-6506.

(48) Frisch, M. J.; Trucks, G. W.; Schlegel, H. B.; Scuseria, G. E.; Robb, M. A.; Cheeseman, J. R.; Scalmani, G.; Barone, V.; Mennucci, B.; Petersson, G. A.; Nakatsuji, H.; Caricato, M.; Li, X.; Hratchian, H. P.; Izmaylov, A. F.; Bloino, J.; Zheng, G.; Sonnenberg, J. L.; Hada, M.; Ehara, M.; Toyota, K.; Fukuda, R.; Hasegawa, J.; Ishida, M.; Nakajima, T.; Honda, Y.; Kitao, O.; Nakai, H.; Vreven, T.; Montgomery, Jr. J. A.; Peralta, J. E.; Ogliaro, F.; Bearpark, M.; Heyd, J. J.; Brothers, E.; Kudin, K. N.; Staroverov, V. N.; Kobayashi, R.; Normand, J.; Raghavachari, K.; Rendell, A.; Burant, J. C.; Iyengar, S. S.; Tomasi, J.; Cossi, M.; Rega, N.; M. Millam, J.; Klene, M.; Knox, J. E.; Cross, J. B.; Bakken, V.; Adamo, C.; Jaramillo, J.; Gomperts, R.; Stratmann, R. E.; Yazyev, O.; Austin, A. J.; Cammi, R.; Pomelli, C.; Ochterski, J.; Martin, R. L.; Morokuma, K.; Zakrzewski, V. G.; Voth, G. A.; Salvador, P.; Dannenberg, J. J.; Dapprich, S.; Daniels, A. D.; Farkas, O.; Foresman, J. B.; Ortiz, J. V.; Cioslowski, J. and J. Fox, D.; Gaussian 09 (Revision E.01), *Gaussian, Inc., Wallingford, CT*, 2013.

(49) Lu, T.; and Chen, F. W.; Multiwfn: A Multifunctional Wavefunction Analyzer. *J. Comp. Chem*., 2012, **33**, 580.